7 SUPPLEMENTARY MATERIALS

7.1 O.O.D GENERALIZATION ERROR BOUND

Denote $\mathbb{E}_p[y|x] := \int_{\mathcal{Y}} yp(y|x)dy$ for any $x, y \in \mathcal{X}\times\mathcal{Y}$. We have $\mathbb{E}_{p^e}[y|s] = \int_{\mathcal{Y}} yp(y|s)dy$ according to that $p(y|s)$ is invariant across $\mathcal{E}$, we can omit p^e in $\mathbb{E}_{p^e}[y|s]$ and denote $g(S) := \mathbb{E}[Y|S]$. Then, the OOD bound $\left|\mathbb{E}_{p^{e_1}}(y|x) - \mathbb{E}_{p^{e_2}}(y|x)\right|$, $\forall(x, y)$ is bounded as follows:

Theorem 7.1 (OOD genearlization error)**.** *Consider two LaCIM P^{e_1} and P^{e_2}, suppose that their densities , i.e., $p^{e_1}(s|x)$ and $p^{e_2}(s|x)$ are absolutely continuous having support $(-\infty, \infty)$. For any $(x, y) \in \mathcal{X} \times \mathcal{Y}$, assume that*

- *$g(S)$ is a Lipschitz-continuous function;*
- *$\pi_x(s) := \frac{p^{e_2}(s|x)}{p^{e_1}(s|x)}$ is differentiable and $\mathbb{E}_{p^{e_1}}\left[\pi_x(S)\middle|g(S) - \mu_1\middle|\right] < \infty$ with $\mu_1 := \mathbb{E}_{p^{e_1}}[g(S)|X = x] = \int_{\mathcal{S}} g(s)p^{e_1}(s|x)ds$;*

then we have $\left|\mathbb{E}_{p^{e_1}}(y|x) - \mathbb{E}_{p^{e_2}}(y|x)\right| \leq \|g'\|_\infty\|\pi'_x\|_\infty \mathrm{Var}_{p^{e_1}}(S|X = x)$.

When $e_1 \in \mathcal{E}_{\text{train}}$ and $e_2 \in \mathcal{E}_{\text{test}}$, the theorem 7.1 describes the error during generalization on e_2 for the strategy that trained on e_1. The bound is mainly affected by: (i) the Lipschitz constant of g, *i.e.*, $\|g\|_\infty$; (ii) $\|\pi'_x\|_\infty$ which measures the difference between $p^{e_1}(s, z)$ and $p^{e_2}(s, z)$; and (iii) the $\mathrm{Var}_{p^{e_1}}(S|x)$ that measures the intensity of $x \to (s, z)$. These terms can be roughly categorized into two classes: (i),(iii) which are related to the property of CIMe and gave few space for improvement; and the (ii) that describes the distributional change between two environments. Specifically for the first class, the (i) measures the smoothness of $\mathbb{E}(y|s)$ with respect to s. The smaller value of $\|g'\|_\infty$ implies that the flatter regions give rise to the same prediction result, hence easier transfer from e_1 to e_2 and vice versa. For the term (iii), consider the deterministic setting that $\varepsilon_x = 0$ (leads to $\mathrm{Var}_{p^{e_1}}(S|x) = 0$), then s can be determined from x for generalization if the f is bijective function.

The term (ii) measures the distributional change between posterior distributions $p^{e_1}(s|x)$ and $p^{e_2}(s|x)$, which contributes to the difference during prediction: $\left|\mathbb{E}_{p^{e_1}}(y|x) - \mathbb{E}_{p^{e_2}}(y|x)\right| = \int_{\mathcal{S}}(p^{e_1}(s|x) - p^{e_1}(s|x))p_{f_y}(y|s)ds$. Such a change is due to the inconsistency between priors $p^{e_1}(s, z)$ and $p^{e_2}(s, z)$, which is caused by different value of the confounder d_s.

Proof. In the following, we will derive the upper bound

$$\left|\mathbb{E}_{p^{e_1}}[Y|X=x] - \mathbb{E}_{p^{e_2}}[Y|X=x]\right| \leq \|g'\|_\infty\|\pi'_x\|_\infty \mathrm{Var}_{p^{e_1}}(S|X = x),$$

where $\pi_x(s) =: \frac{p^{e_2}(s|x)}{p^{e_1}(s|x)}$ and $g(s)$ is assumed to be Lipschitz-continuous.

To begin with, note that

$$\mathbb{E}[Y|X] = \mathbb{E}[\mathbb{E}(Y|X, S)|X] = \mathbb{E}[g(S)|X] = \int g(s)p(s|x)ds.$$

Let $p_1(s|x) = p^{e_1}(s|x)$, $p_2(s|x) = p^{e_2}(s|x)$. For ease of notations, we use P_1 and P_2 denote the distributions with densities $p_1(s|x)$ and $p_2(s|x)$ and suppose $S_1 \sim P_1$ and $S_2 \sim P_2$, where x is omitted as the following analysis is conditional on a fixed $X=x$.

Then we may rewrite the difference of conditional expectations as

$$\mathbb{E}_{p^{e_2}}[Y|X = x] - \mathbb{E}_{p^{e_1}}[Y|X = x] = \mathbb{E}(g(S_2)) - \mathbb{E}(g(S_1)),$$

where $\mathbb{E}[g(S_j))] = \int g(s)p_j(s|x)ds$ denotes the expectation over P_j.

Let $\mu_1 := \mathbb{E}_{p^{e_1}}[g(S)|X = x] = \mathbb{E}[g(S_1)] = \int g(s)p_1(s|x)ds$. Then

$$\mathbb{E}_{p^{e_2}}[Y|X = x] - \mathbb{E}_{p^{e_1}}[Y|X = x] = \mathbb{E}(g(S_2)) - \mathbb{E}(g(S_1)) = \mathbb{E}[g(S_2) - \mu_1].$$

Further, we have the following transformation

$$\mathbb{E}[g(S_2) - \mu_1] = \int (g(s) - \mu_1)\pi_x(s)p_1(s|x)ds = \mathbb{E}[(g(S_1) - \mu_1)\pi_x(S_1)]. \tag{3}$$

In the following, we will use the results of the Stein kernel function. Please refer to Definition 7.2 for a general definition. Particularly, for the distribution $P_1 \sim p_1(s|x)$, the Stein kernel $\tau_1(s)$ is

$$\tau_1(s) = \frac{1}{p_1(s|x)} \int_{-\infty}^{s} (\mathbb{E}(S_1) - t) p_1(t|x) dt, \tag{4}$$

where $\mathbb{E}(S_1) = \int s \cdot p_1(s|x) ds$. Further, we define $(\tau_1 \circ g)(s)$ as

$$(\tau_1 \circ g)(s) = \frac{1}{p_1(s|x)} \int_{-\infty}^{s} (\mathbb{E}(g(S_1)) - g(t)) p_1(t|x) dt = \frac{1}{p_1(s|x)} \int_{-\infty}^{s} (\mu_1 - g(t)) p_1(t|x) dt. \tag{5}$$

Under the second condition listed in Theorem 7.1, we may apply the result of Lemma 7.3. Specifically, by the equation (8), we have

$$\mathbb{E}\left[(g(S_1) - \mu_1)\pi_x(S_1)\right] = \mathbb{E}\left[(\tau_1 \circ g)(S_1)\pi_x'(S_1)\right].$$

Then under the first condition in Theorem 7.1, we can obtain the following inequality by Lemma 7.4,

$$\begin{aligned} \mathbb{E}\left[(\tau_1 \circ g)(S_1)\pi_x'(S_1)\right] &= \mathbb{E}\left[\left(\frac{(\tau_1 \circ g)}{\tau_1}\pi_x'\tau_1\right)(S_1)\right] \leq \mathbb{E}\left[\left|\frac{(\tau_1 \circ g)}{\tau_1}(S_1)\right| \cdot \left|\pi_x'\tau_1(S_1)\right|\right] \\ &\leq \|g'\|_\infty \mathbb{E}\left[\left|\left(\pi_x'\tau_1\right)(S_1)\right|\right] \leq \|g'\|_\infty \|\pi_x'\|_\infty \mathbb{E}\left[|\tau_1(S_1)|\right]. \end{aligned} \tag{6}$$

In the following, we show that the Stein kernel is non-negative, which enables $\mathbb{E}\left[|\tau_1(S_1)|\right] = \mathbb{E}\left[\tau_1(S_1)\right]$. According to the definition, $\tau_1(s) = \frac{1}{p_1(s|x)} \int_{-\infty}^{s} (\mathbb{E}(S_1) - t) p_1(t|x) dt$, where $\mathbb{E}(S_1) = \int_{-\infty}^{\infty} t \cdot p_1(t|x) dt$. Let $F_1(s) = \int_{-\infty}^{s} p_1(t|x) dt$ be the distribution function for P_1. Note that

$$\begin{aligned} \int_{-\infty}^{s} \mathbb{E}(S_1) p_1(t|x) dt &= F_1(s)\mathbb{E}(S_1) = F_1(s)\,\mathrm{E}(S_1), \\ \int_{-\infty}^{s} t p_1(t|x) dt &= F_1(s) \int_{-\infty}^{s} t \frac{p_1(t|x)}{F_1(s)} dt = F_1(s)\,\mathrm{E}(S_1|S_1 \leq s) \leq F_1(s)\,\mathrm{E}(S_1), \end{aligned}$$

The last inequality is based on $\mathrm{E}(S_1|S_1 \leq s) - \mathrm{E}(S_1) \leq 0$ that can be proved as the following

$$\begin{aligned} \int_{-\infty}^{s} t \frac{p_1(t|x)}{F_1(s)} dt - \int_{-\infty}^{\infty} t p_1(t|x) dt &= \int_{-\infty}^{s} t \left(\frac{1}{F_1(s)} - 1\right) p_1(t|x) dt - \int_{s}^{\infty} t p_1(t|x) dt \\ &\leq s \int_{-\infty}^{s} \left(\frac{1}{F_1(s)} - 1\right) p_1(t|x) dt - s \int_{s}^{\infty} p_1(t|x) = 0. \end{aligned}$$

Therefore, $\tau_1(s) \geq 0$ and hence $\mathbb{E}\left[|\tau_1(S_1)|\right] = \mathbb{E}\left[\tau_1(S_1)\right]$ in (6).

Besides, by equation (9), the special case of Lemma 7.3, we have

$$\mathbb{E}\left[\tau_1(S_1)\right] = \mathrm{Var}(S_1) = \mathrm{Var}_{p^{e_1}}(S|X = x).$$

To sum up,

$$\mathbb{E}\left[(\tau_1 \circ g)(S_1)\pi_x'(S_1)\right] \leq \|g'\|_\infty \|\pi_x\|_\infty \mathbb{E}\left[\tau_1(S_1)\right] = \|g'\|_\infty \|\pi_x'\|_\infty \mathrm{Var}_{p^{e_1}}(S|X = x).$$

□

Definition 7.2 (the Stein Kernel τ_P of distribution P). Suppose $X \sim P$ with density p. The Stein kernel of P is the function $x \mapsto \tau_P(x)$ defined by

$$\tau_P(x) = \frac{1}{p(x)} \int_{-\infty}^{x} (\mathbb{E}(X) - y) p(y) dy, \tag{7}$$

where Id is the identity function for $\mathrm{Id}(x) = x$. More generally, for a function h satisfying $\mathbb{E}[|h(X)|] < \infty$, define $(\tau_P \circ h)(x)$ as

$$(\tau_P \circ h)(x) = \frac{1}{p(x)} \int_{-\infty}^{x} (\mathbb{E}(h(X)) - h(y)) p(y) dy.$$

Lemma 7.3. *For a differentiable function φ such that $\mathbb{E}[|(\tau_P \circ h)(x)\varphi'(X)|] < \infty$, we have*

$$\mathbb{E}\left[(\tau_P \circ h)(x)\varphi'(X)\right] = \mathbb{E}[(h(X) - \mathbb{E}(h(X))\varphi(X)]. \tag{8}$$

Proof. Let $\mu_h =: \mathbb{E}(h(X))$. As $\mathbb{E}(h(X) - \mu_h) = 0$,

$$(\tau_P \circ h)(x) = \frac{1}{p(x)} \int_{-\infty}^{x} (\mu_h - h(y))p(y)dy = \frac{-1}{p(x)} \int_{x}^{\infty} (\mu_h - h(y))p(y)dy.$$

Then

$$\begin{aligned}
\mathbb{E}\left[(\tau_P \circ h)(x)\varphi'(X)\right] &= \int_{-\infty}^{0} (\tau_P \circ h)(x)\varphi'(x)p(x)dx + \int_{0}^{\infty} (\tau_P \circ h)(x)\varphi'(x)p(x)dx \\
&= \int_{-\infty}^{0}\int_{-\infty}^{x} (\mu_h - h(y))p(y)\varphi'(x)dydx - \int_{0}^{\infty}\int_{x}^{\infty} (\mu_h - h(y))p(y)\varphi'(x)dydx \\
&= \int_{-\infty}^{0}\int_{y}^{0} (\mu_h - h(y))p(y)\varphi'(x)dxdy - \int_{0}^{\infty}\int_{0}^{y} (\mu_h - h(y))p(y)\varphi'(x)dxdy \\
&= \int_{-\infty}^{0}\int_{0}^{y} (h(y) - \mu_h)p(y)\varphi'(x)dxdy + \int_{0}^{\infty}\int_{0}^{y} (h(y) - \mu_h)p(y)\varphi'(x)dxdy \\
&= \int_{-\infty}^{\infty} (h(y) - \mu_h)p(y)\left(\int_{0}^{y} \varphi'(x)dx\right)dy = \int_{-\infty}^{\infty} (h(y) - \mu_h)p(y)(\varphi(y) - \varphi(0))dy \\
&= \int_{-\infty}^{\infty} (h(y) - \mu_h)p(y)(\varphi(y))dy = \mathbb{E}[(h(X) - \mathbb{E}(h(X))\varphi(X)]
\end{aligned}$$

Particularly, taking $h(X) = X$ and $\varphi(X) = X - \mathbb{E}(X)$, we immediately have

$$\mathbb{E}(\tau_P(X)) = \mathrm{Var}(X) \tag{9}$$

□

Lemma 7.4. *Assume that $\mathbb{E}(|X|) < \infty$ and the density p is locally absolutely continuous on $(-\infty, \infty)$ and h is a Lipschitz continuous function. Then we have $|f_h| \leq \|h'\|_\infty$ for*

$$f_h(x) = \frac{(\tau_P \circ h)(x)}{\tau_P(x)} = \frac{\int_{-\infty}^{x}(\mathbb{E}(h(X)) - h(y))p(y)dy}{\int_{-\infty}^{x}(\mathbb{E}(X) - y)p(y)dy}.$$

Proof. This is a special case of Corollary 3.15 in Döbler et al. (2015), taking the constant $c = 1$. □

7.2 Proof of the Equivalence of Definition 4.2

Proposition 7.5. *The binary relation $\sim_p$ defined in Def. 4.2 is an equivalence relation.*

Proof. The equivalence relation should satisfy three properties as follows:

- *Reflexive* property: The $\theta \sim_p \theta$ with M_z, M_s being identity matrix and a_s, a_z being 0.
- *Symmtric* property: If $\theta \sim_p \tilde{\theta}$, then there exists block permutation matrices M_z and M_s such that

  $$\mathbf{T}^s([f_x]_{\mathcal{S}}^{-1}(x)) = M_s\tilde{\mathbf{T}}^s([\tilde{f}_x]_{\mathcal{S}}^{-1}(x)) + a_s,\ \mathbf{T}^z([f_x]_{\mathcal{Z}}^{-1}(x)) = M_z\tilde{\mathbf{T}}^z([\tilde{f}_x]_{\mathcal{Z}}^{-1}(x)) + a_z,$$
  $$p_{f_y}(y|[f_x]_{\mathcal{S}}^{-1}(x)) = p_{\tilde{f}_y}(y|[\tilde{f}_x]_{\mathcal{S}}^{-1}(x)).$$

  The we have M_s^{-1} and M_z^{-1} are also block permutation matrices and such that:

  $$\tilde{\mathbf{T}}^s([\tilde{f}_x]_{\mathcal{S}}^{-1}(x)) = M_s^{-1}\mathbf{T}^s([f_x]_{\mathcal{S}}^{-1}(x)) + (-a_s),\ \tilde{\mathbf{T}}^s([\tilde{f}_x]_{\mathcal{Z}}^{-1}(x)) = M_z^{-1}\mathbf{T}^s([f_x]_{\mathcal{Z}}^{-1}(x)) + (-a_z),$$
  $$p_{\tilde{f}_y}(y|[\tilde{f}_x]_{\mathcal{S}}^{-1}(x)) = p_{f_y}(y|[f_x]_{\mathcal{S}}^{-1}(x)).$$

  Therefore, we have $\tilde{\theta} \sim_p \theta$.

- *Transitive* property: if $\theta_1 \sim_p \theta_2$ and $\theta_2 \sim_p \theta_3$ with $\theta_i := \{f_x^i, f_y^i, \mathbf{T}^{s,1}, \mathbf{T}^{z,1}, \mathbf{\Gamma}^{s,i}, \mathbf{\Gamma}^{z,i}\}$, then we have

$$\begin{aligned}
\mathbf{T}^{s,1}((f_{x,s}^1)^{-1}(x)) &= M_s^1 \mathbf{T}^{s,2}((f_{x,s}^2)^{-1}(x)) + a_s^1, \\
\mathbf{T}^{z,1}((f_{x,z}^1)^{-1}(x)) &= M_z^1 \mathbf{T}^{z,2}((f_{x,z}^2)^{-1}(x)) + a_z^2, \\
\mathbf{T}^{s,2}((f_{x,s}^2)^{-1}(x)) &= M_s^2 \mathbf{T}^{s,3}((f_{x,s}^3)^{-1}(x)) + a_s^2, \\
\mathbf{T}^{z,2}((f_{x,z}^2)^{-1}(x)) &= M_z^2 \mathbf{T}^{z,3}((f_z^3)^{-1}(x)) + a_{x,z}^3
\end{aligned}$$

for block permutation matrices $M_s^1, M_z^1, M_s^2, M_z^2$ and vectors $a_s^1, a_s^2, a_z^1, a_z^2$. Then we have

$$\begin{aligned}
\mathbf{T}^{s,1}((f_{x,s}^1)^{-1}(x)) &= M_s^2 M_s^1 \mathbf{T}^{s,3}((f_{x,s}^3)^{-1}(x)) + (M_s^2 a_s^1) + a_s^2, \\
\mathbf{T}^{z,1}((f_{x,z}^1)^{-1}(x)) &= M_z^2 M_z^1 \mathbf{T}^{z,3}((f_{x,z}^3)^{-1}(x)) + (M_z^2 a_z^1) + a_z^2.
\end{aligned}$$

Besides, it is apparent that

$$p_{f_y^1}(y|(f_x^1)_s^{-1}(x)) = p_{f_y^2}(y|(f_x^2)_s^{-1}(x)) = p_{f_y^3}(y|(f_x^3)_s^{-1}(x)). \tag{10}$$

Therefore, we have $\theta_1 \sim_p \theta_3$ since $M_s^2 M_s^1$ and $M_z^2 M_z^1$ are also permutation matrices.

With above three properties satisfied, we have that $\sim_p$ is a equivalence relation. □

7.3 Proof of Theorem 4.3

In the following, we write $p^e(x, y)$ as $p(x, y|d^e)$ and also $\Gamma_c^{t=s,z} := \Gamma^{t=s,z}(d^e), S_{c,i} = S_i(d^e), Z_{c,i} = Z_i(d^e)$. To prove the theorem 4.3, we first prove the theorem 7.6 for the simplest case when $c|d^e = d^e$, then we generalize to the case when $\mathcal{C} := \cup_r \mathcal{C}_r$. The overall roadmap is as follows: we first prove the $\sim_A$-identifiability in theorem 7.9, and the combination of which with lemma 7.12, 7.11 give theorem 7.6 in the simplest case when $c|d^e = d^e$. Then we generalize the case considered in theorem 7.6 to the more general case when $\mathcal{C} := \cup_r \mathcal{C}_r$.

Theorem 7.6 ($\sim_p$-identifiability). *For θ in the LaCIM $p_\theta^e(x, y) \in \mathcal{P}_{\text{exp}}$ for any $e \in \mathcal{E}_{\text{train}}$, we assume that* **(1)** *the CIMe satisfies that f_x, f_x' and f_x'' are continuous and that f_x, f_y are bijective;* **(2)** *that the $T_{i,j}^t$ are twice differentiable for any $t = s, z, i \in [q_t], j \in [k_t]$;* **(3)** *the exogenous variables satisfy that the characteristic functions of $\varepsilon_x, \varepsilon_y$ are almost everywhere nonzero;* **(4)** *the number of environments, i.e., $m \geq \max(q_s * k_s, q_z * k_z) + 1$ and $\left[\mathbf{\Gamma}_{d^{e_2}}^{t=s,z} - \mathbf{\Gamma}_{d^{e_1}}^{t=s,z}, ..., \mathbf{\Gamma}_{d^{e_m}}^{t=s,z} - \mathbf{\Gamma}_{d^{e_1}}^{t=s,z}\right]$ have full column rank for both $t = s$ and $t = z$, we have that the parameters $\theta := \{f_x, f_y, \mathbf{T}^s, \mathbf{T}^z\}$ are $\sim_p$ identifiable.*

To prove theorem 7.6, We first prove the $\sim_A$-identifiability that is defined as follows:

Definition 7.7 ($\sim_A$-identifiability). *The definition is the same with the one defined in 4.2, with M_s, M_z being invertible matrices which are not necessarily to be the permutation matrices in Def. 4.2.*

Proposition 7.8. *The binary relation $\sim_A$ defined in Def. 7.7 is an equivalence relation.*

Proof. The proof is similar to that of proposition 7.5. □

The following theorem states that any LaCIM that belongs to $\mathcal{P}_{\text{exp}}$ is $\sim_A$-identifiable.

Theorem 7.9 ($\sim_A$-identifiability). *For θ in the LaCIM $p_\theta^e(x, y) \in \mathcal{P}_{\text{exp}}$ for any $e \in \mathcal{E}_{\text{train}}$, we assume* **(1)** *the CIMe satisfies that f_x, f_y are bijective;* **(2)** *the $T_{i,j}^t$ are twice differentiable for any $t = s, z, i \in [q_t], j \in [k_t]$;* **(3)** *the exogenous variables satisfy that the characteristic functions of $\varepsilon_x, \varepsilon_y$ are almost everywhere nonzero;* **(4)** *the number of environments, i.e., $m \geq \max(q_s * k_s, q_z * k_z) + 1$ and $\left[[\mathbf{\Gamma}_{d^{e_2}}^t - \mathbf{\Gamma}_{d^{e_1}}^t]^\mathsf{T}, ..., [\mathbf{\Gamma}_{d^{e_m}}^t - \mathbf{\Gamma}_{d^{e_1}}^t]^\mathsf{T}\right]^\mathsf{T}$ have full column rank for $t = s, z$, we have that the parameters $\{f_x, f_y, \mathbf{T}^s, \mathbf{T}^z\}$ are $\sim_p$ identifiable.*

Proof. Suppose that $\theta = \{f_x, f_y, \mathbf{T}^s, \mathbf{T}^z\}$ and $\tilde{\theta} = \{\tilde{f}_x, \tilde{g}_y, \tilde{\mathbf{T}}^s, \tilde{\mathbf{T}}^z\}$ share the same observational distribution for each environment $e \in \mathcal{E}_{\text{train}}$, *i.e.*,

$$p_{f_x, f_y, \mathbf{T}^s, \mathbf{\Gamma}^s, \mathbf{T}^z, \mathbf{\Gamma}^z}(x, y|d^e) = p_{\tilde{f}_x, \tilde{f}_y, \tilde{\mathbf{T}}^s, \tilde{\mathbf{\Gamma}}^s, \tilde{\mathbf{T}}^z, \tilde{\mathbf{\Gamma}}^z}(x, y|d^e). \tag{11}$$

Then we have

$$p_{f_x,f_y,\mathbf{T}^s,\mathbf{\Gamma}^s,\mathbf{T}^z,\mathbf{\Gamma}^z}(x|d^e) = p_{\tilde{f}_x,\tilde{f}_y,\tilde{\mathbf{T}}^s,\tilde{\mathbf{\Gamma}}^s,\tilde{\mathbf{T}}^z,\tilde{\mathbf{\Gamma}}^z}(x|d^e) \tag{12}$$

$$\implies \int_{\mathcal{S}\times\mathcal{Z}} p_{f_x}(x|s,z)p_{\mathbf{T}^s,\mathbf{\Gamma}^s,\mathbf{T}^z,\mathbf{\Gamma}^z}(s,z|d^e)dsdz = \int_{\mathcal{S}\times\mathcal{Z}} p_{\tilde{f}_x}(x|s,z)p_{\tilde{\mathbf{T}}^s,\tilde{\mathbf{\Gamma}}^s,\tilde{\mathbf{T}}^z,\tilde{\mathbf{\Gamma}}^z}(s,z|d^e)dsdz \tag{13}$$

$$\implies \int_{\mathcal{X}} p_{\varepsilon_x}(x-\bar{x})p_{\mathbf{T}^s,\mathbf{\Gamma}^s,\mathbf{T}^z,\mathbf{\Gamma}^z}(f_x^{-1}(\bar{x})|d^e)\mathrm{vol}J_{f_x^{-1}}(\bar{x})d\bar{x} \tag{14}$$

$$= \int_{\mathcal{X}} p_{\varepsilon_x}(x-\bar{x})p_{\tilde{\mathbf{T}}^s,\tilde{\mathbf{\Gamma}}^s,\tilde{\mathbf{T}}^z,\tilde{\mathbf{\Gamma}}^z}(\tilde{f}_x^{-1}(\bar{x})|d^e)\mathrm{vol}J_{\tilde{f}_x^{-1}}(\bar{x})d\bar{x} \tag{15}$$

$$\implies \int_{\mathcal{X}} \tilde{p}_{\mathbf{T}^s,\mathbf{\Gamma}^s,\mathbf{T}^z,\mathbf{\Gamma}^z,f_x}(\bar{x}|d^e)p_{\varepsilon_x}(x-\bar{x})d\bar{x} = \int_{\mathcal{X}} \tilde{p}_{\tilde{\mathbf{T}}^s,\tilde{\mathbf{\Gamma}}^s,\tilde{\mathbf{T}}^z,\tilde{\mathbf{\Gamma}}^z,\tilde{f}_x}(\bar{x}|d^e)p_{\varepsilon_x}(x-\bar{x})d\bar{x} \tag{16}$$

$$\implies (\tilde{p}_{\mathbf{T}^s,\mathbf{\Gamma}^s,\mathbf{T}^z,\mathbf{\Gamma}^z,f_x} * p_{\varepsilon_x})(x|d^e) = (\tilde{p}_{\tilde{\mathbf{T}}^s,\tilde{\mathbf{\Gamma}}^s,\tilde{\mathbf{T}}^z,\tilde{\mathbf{\Gamma}}^z,\tilde{f}_x}) * p_{\varepsilon_x}(x|d^e) \tag{17}$$

$$\implies F[\tilde{p}_{\mathbf{T}^s,\mathbf{\Gamma}^s,\mathbf{T}^z,\mathbf{\Gamma}^z,f_x}](\omega)\varphi_{\varepsilon_x}(\omega) = F[\tilde{p}_{\tilde{\mathbf{T}}^s,\tilde{\mathbf{\Gamma}}^s,\tilde{\mathbf{T}}^z,\tilde{\mathbf{\Gamma}}^z,\tilde{f}_x}](\omega)\varphi_{\varepsilon_x}(\omega) \tag{18}$$

$$\implies F[\tilde{p}_{\mathbf{T}^s,\mathbf{\Gamma}^s,\mathbf{T}^z,\mathbf{\Gamma}^z,f_x}](\omega) = F[\tilde{p}_{\tilde{\mathbf{T}}^s,\tilde{\mathbf{\Gamma}}^s,\tilde{\mathbf{T}}^z,\tilde{\mathbf{\Gamma}}^z,\tilde{f}_x}](\omega) \tag{19}$$

$$\implies \tilde{p}_{\mathbf{T}^s,\mathbf{\Gamma}^s,\mathbf{T}^z,\mathbf{\Gamma}^z,f_x}(x|d^e) = \tilde{p}_{\tilde{\mathbf{T}}^s,\tilde{\mathbf{\Gamma}}^s,\tilde{\mathbf{T}}^z,\tilde{\mathbf{\Gamma}}^z,\tilde{f}_x}(x|d^e) \tag{20}$$

where $\mathrm{vol}J_f(X) := \det(J_f(X))$ for any square matrix X and function f with "J" standing for the Jacobian. The $\tilde{p}_{\mathbf{T}^s,\mathbf{\Gamma}^s,\mathbf{T}^z,\mathbf{\Gamma}^z,f_x}(x)$ in Eq. (16) is denoted as $p_{\mathbf{T}^s,\mathbf{\Gamma}^s,\mathbf{T}^z,\mathbf{\Gamma}^z}(f_x^{-1}(x|d^e)\mathrm{vol}J_{f^{-1}}(x)$. The '$*$' in Eq. (17) denotes the convolution operator. The $F[\cdot]$ in Eq. (18) denotes the Fourier transform, where $\phi_{\varepsilon_x}(\omega) = F[p_{\varepsilon_x}](\omega)$. Since we assume that the $\varphi_{\varepsilon_x}(\omega)$ is non-zero almost everywhere, we can drop it to get Eq. (20). Similarly, we have that:

$$p_{f_y,\mathbf{T}^s,\mathbf{\Gamma}^s}(y|d^e) = p_{\tilde{f}_y,\tilde{\mathbf{T}}^s,\tilde{\mathbf{\Gamma}}^s}(y|d^e) \tag{21}$$

$$\implies \int_{\mathcal{S}} p_{f_y}(y|s)p_{\mathbf{T}^s,\mathbf{\Gamma}^s}(s|d^e)ds = \int_{\mathcal{S}} p_{\tilde{f}_y}(y|s)p_{\tilde{\mathbf{T}}^s,\tilde{\mathbf{\Gamma}}^s}(s|d^e)ds \tag{22}$$

$$\implies \int_{\mathcal{Y}} p_{\varepsilon_y}(y-\bar{y})p_{\mathbf{T}^s,\mathbf{\Gamma}^s}(f_y^{-1}(\bar{y})|d^e)\mathrm{vol}J_{f_y^{-1}}(\bar{y})d\bar{y} \tag{23}$$

$$= \int_{\mathcal{Y}} p_{\varepsilon_y}(y-\bar{y})p_{\tilde{\mathbf{T}}^s,\tilde{\mathbf{\Gamma}}^s}(\tilde{f}_y^{-1}(\bar{y})|d^e)\mathrm{vol}J_{\tilde{g}^{-1}}(\bar{y})d\bar{y} \tag{24}$$

$$\implies \int_{\mathcal{S}} \tilde{p}_{\mathbf{T}^s,\mathbf{\Gamma}^s,f_y}(\bar{y}|d^e)p_{\varepsilon_y}(y-\bar{y})d\bar{y} = \int_{\mathcal{S}} \tilde{p}_{\tilde{\mathbf{T}}^s,\tilde{\mathbf{\Gamma}}^s,\tilde{f}_y}(\bar{y}|d^e)p_{\varepsilon_y}(y-\bar{y})d\bar{y} \tag{25}$$

$$\implies (\tilde{p}_{\mathbf{T}^s,\mathbf{\Gamma}^s,f_y} * p_{\varepsilon_y})(y|d^e) = (\tilde{p}_{\tilde{\mathbf{T}}^s,\tilde{\mathbf{\Gamma}}^s,\tilde{f}_y} * p_{\varepsilon_y})(y|d^e) \tag{26}$$

$$\implies F[\tilde{p}_{\mathbf{T}^s,\mathbf{\Gamma}^s,f_y}](\omega)\varphi_{\varepsilon_y}(\omega) = F[\tilde{p}_{\tilde{\mathbf{T}}^s,\tilde{\mathbf{\Gamma}}^s,\tilde{f}_y}](\omega)\varphi_{\varepsilon_y}(\omega) \tag{27}$$

$$\implies F[\tilde{p}_{\mathbf{T}^s,\mathbf{\Gamma}^s,f_y}](\omega) = F[\tilde{p}_{\tilde{\mathbf{T}}^s,\tilde{\mathbf{\Gamma}}^s,\tilde{f}_y}](\omega) \tag{28}$$

$$\implies \tilde{p}_{\mathbf{T}^s,\mathbf{\Gamma}^s,f_y}(y) = \tilde{p}_{\mathbf{T}^s,\mathbf{\Gamma}^s,\tilde{f}_y}(y), \tag{29}$$

and that

$$p_{f_x,f_y\mathbf{T}^s,\mathbf{\Gamma}^s,\mathbf{T}^z,\mathbf{\Gamma}^z}(x,y|d^e) = p_{\tilde{f}_x,\tilde{f}_y,\tilde{\mathbf{T}}^s,\tilde{\mathbf{\Gamma}}^s,\tilde{\mathbf{T}}^z,\tilde{\mathbf{\Gamma}}^z}(x,y|d^e) \tag{30}$$

$$\implies \int_{\mathcal{S}\times\mathcal{Z}} p_{f_x}(x|s,z)p_{f_y}(y|s)p_{\mathbf{T}^s,\mathbf{\Gamma}^s,\mathbf{T}^z,\mathbf{\Gamma}^z}(s,z|d^e)dsdz$$

$$= \int_{\mathcal{S}\times\mathcal{Z}} p_{\tilde{f}}(x|s,z)p_{\tilde{f}_y}(y|s)p_{\tilde{\mathbf{T}}^s,\tilde{\mathbf{\Gamma}}^s,\tilde{\mathbf{T}}^z,\tilde{\mathbf{\Gamma}}^z}(s,z|d^e)dsdz \tag{31}$$

$$\implies \int_{\mathcal{V}} p_{\varepsilon}(v-\bar{v})p_{\mathbf{T}^s,\mathbf{\Gamma}^s,\mathbf{T}^z,\mathbf{\Gamma}^z}(h^{-1}(\bar{v})|d^e)\mathrm{vol}J_{h^{-1}}(\bar{v})d\bar{v} \tag{32}$$

$$= \int_{\mathcal{V}} p_{\varepsilon}(v-\bar{v})p_{\tilde{\mathbf{T}}^s,\tilde{\mathbf{\Gamma}}^s,\tilde{\mathbf{T}}^z,\tilde{\mathbf{\Gamma}}^z}(\tilde{h}^{-1}(\bar{v})|d^e)\mathrm{vol}J_{\tilde{h}^{-1}}(\bar{v})d\bar{v} \tag{33}$$

$$\implies \int_{\mathcal{S}\times\mathcal{Z}} \tilde{p}_{\mathbf{T}^s,\mathbf{\Gamma}^s,\mathbf{T}^z,\mathbf{\Gamma}^z,h,c}(\bar{v}|d)p_{\varepsilon}(v-\bar{v})d\bar{v} = \int_{\mathcal{S}\times\mathcal{Z}} \tilde{p}_{\tilde{\mathbf{T}}^s,\tilde{\mathbf{\Gamma}}^s,\tilde{\mathbf{T}}^z,\tilde{\mathbf{\Gamma}}^z,\tilde{h},d^e}(\bar{v}|d^e)p_{\varepsilon}(v-\bar{v})d\bar{v} \tag{34}$$

$$\implies (\tilde{p}_{\mathbf{T}^s,\mathbf{\Gamma}^s,\mathbf{T}^z,\mathbf{\Gamma}^z,h} * p_{\varepsilon})(v) = (\tilde{p}_{\tilde{\mathbf{T}}^s,\tilde{\mathbf{\Gamma}}^s,\tilde{\mathbf{T}}^z,\tilde{\mathbf{\Gamma}}^z,\tilde{h}} * p_{\varepsilon})(v) \tag{35}$$

$$\Longrightarrow F[\tilde{p}_{\mathbf{T}^s,\mathbf{\Gamma}^s,\mathbf{T}^z,\mathbf{\Gamma}^z,h}](\omega)\varphi_\varepsilon(\omega) = F[\tilde{p}_{\tilde{\mathbf{T}}^s,\tilde{\mathbf{\Gamma}}^s,\tilde{\mathbf{T}}^z,\tilde{\mathbf{\Gamma}}^z,\tilde{h}}](\omega)\varphi_\varepsilon(\omega) \tag{36}$$

$$\Longrightarrow F[\tilde{p}_{\mathbf{T}^s,\mathbf{\Gamma}^s,\mathbf{T}^z,\mathbf{\Gamma}^z,h}](\omega) = F[\tilde{p}_{\tilde{\mathbf{T}}^s,\tilde{\mathbf{\Gamma}}^s,\tilde{\mathbf{T}}^z,\tilde{\mathbf{\Gamma}}^z,\tilde{h}}](\omega) \tag{37}$$

$$\Longrightarrow \tilde{p}_{\mathbf{T}^s,\mathbf{\Gamma}^s,\mathbf{T}^z,\mathbf{\Gamma}^z,h}(v) = \tilde{p}_{\mathbf{T}^s,\mathbf{\Gamma}^s,\mathbf{T}^z,\mathbf{\Gamma}^z,h}(v), \tag{38}$$

where $v := [x^\top, y^\top]^\top$, $\varepsilon := [\varepsilon_x^\top, \varepsilon_y^\top]^\top$, $h(v) = [[f_x]_{\mathcal{Z}}^{-1}(x)^\top, f_y^{-1}(y)^\top]^\top$. According to Eq. (29), we have

$$\begin{aligned}
&\log \mathrm{vol} J_{f_y}(y) + \sum_{i=1}^{q_s}\left(\log B_i(f_{y,i}^{-1}(y)) - \log A_i(d^e) + \sum_{j=1}^{k_s} T_{i,j}^s(f_{y,i}^{-1}(y))\Gamma_{i,j}^s(d^e)\right) \\
&\qquad = \log \mathrm{vol} J_{\tilde{f}_y}(y) + \sum_{i=1}^{q_s}\left(\log \tilde{B}_i(\tilde{f}_{y,i}^{-1}(y)) - \log \tilde{A}_i(d^e) + \sum_{j=1}^{k_s} \tilde{T}_{i,j}^s(\tilde{f}_{y,i}^{-1}(y))\tilde{\Gamma}_{i,j}^s(d^e)\right)
\end{aligned} \tag{39}$$

Suppose that the assumption (4) holds, then we have

$$\langle \mathbf{T}^s(f_y^{-1}(y)), \overline{\mathbf{\Gamma}}^s(d^{e_k})\rangle + \sum_i \log \frac{A_i(d^{e_1})}{A_i(d^{e_k})} = \langle \tilde{\mathbf{T}}^s(\tilde{f}_y^{-1}(y)), \overline{\tilde{\mathbf{\Gamma}}}^s(d^{e_k})\rangle + \sum_i \log \frac{\tilde{A}_i(d^{e_1})}{\tilde{A}_i(d^{e_k})} \tag{40}$$

for all $k \in [m]$, where $\bar{\mathbf{\Gamma}}(d) = \mathbf{\Gamma}(d) - \mathbf{\Gamma}(d^{e_1})$. Denote $\tilde{b}_s(k) = \sum_i \frac{\tilde{A}_i(d^{e_1})A_i(d^{e_k})}{\tilde{A}_i(d^{e_k})A_i(d^{e_1})}$ for $k \in [m]$, then we have

$$\overline{\mathbf{\Gamma}}^{s,\top}\mathbf{T}^s(f_y^{-1}(y)) = \overline{\tilde{\mathbf{\Gamma}}}^{s,\top}\tilde{\mathbf{T}}^s(\tilde{f}_y^{-1}(y)) + \tilde{b}_s, \tag{41}$$

Similarly, from Eq. (20) and Eq. (38), there exists $\tilde{b}_z, \tilde{b}_s$ such that

$$\overline{\mathbf{\Gamma}}^{s,\top}\mathbf{T}^s([f_x]_{\mathcal{S}}^{-1}(x)) + \overline{\mathbf{\Gamma}}^{z,\top}\mathbf{T}^z([f_x]_{\mathcal{Z}}^{-1}(x)) = \overline{\tilde{\mathbf{\Gamma}}}^{s,\top}\tilde{\mathbf{T}}^s([\tilde{f}_x]_{\mathcal{S}}^{-1}(x)) + \overline{\tilde{\mathbf{\Gamma}}}^{z,\top}\tilde{\mathbf{T}}^z([\tilde{f}_x]_{\mathcal{Z}}^{-1}(x)) + \tilde{b}_z + \tilde{b}_s, \tag{42}$$

where $\tilde{b}_z(k) = \sum_i \frac{\tilde{Z}_i(d^{e_1})Z_i(d^{e_k})}{\tilde{Z}_i(d^{e_k})Z_i(d^{e_1})}$ for $k \in [m]$; and that,

$$\overline{\mathbf{\Gamma}}^{s,\top}\mathbf{T}^s(f_y^{-1}(y)) + \overline{\mathbf{\Gamma}}^{z,\top}\mathbf{T}^z([f_x^{-1}]_{\mathcal{Z}}(x)) = \overline{\tilde{\mathbf{\Gamma}}}^{s,\top}\tilde{\mathbf{T}}^s(\tilde{f}_y^{-1}(y)) + \overline{\tilde{\mathbf{\Gamma}}}^{z,\top}\tilde{\mathbf{T}}^z([\tilde{f}_x^{-1}]_{\mathcal{Z}}(x)) + \tilde{b}_z + \tilde{b}_s. \tag{43}$$

Substituting Eq. (41) to Eq. (42) and Eq. (43), we have that

$$\overline{\mathbf{\Gamma}}^{z,\top}\mathbf{T}^z([f_x^{-1}]_{\mathcal{Z}}(y)) = \overline{\tilde{\mathbf{\Gamma}}}^{z,\top}\tilde{\mathbf{T}}^z([\tilde{f}_x^{-1}]_{\mathcal{Z}}(y)) + \tilde{b}_z,\ \overline{\mathbf{\Gamma}}^{s,\top}\mathbf{T}^s([f_x^{-1}]_{\mathcal{S}}(y)) = \overline{\tilde{\mathbf{\Gamma}}}^{s,\top}\tilde{\mathbf{T}}^s([\tilde{f}_x^{-1}]_{\mathcal{S}}(y)) + \tilde{b}_s. \tag{44}$$

According to assumption (4), the $\overline{\mathbf{\Gamma}}^{s,\top}$ and $\overline{\mathbf{\Gamma}}^{z,\top}$ have full column rank. Therefore, we have that

$$\mathbf{T}^z([f_x^{-1}]_{\mathcal{Z}}(x)) = \left(\overline{\mathbf{\Gamma}}^z\overline{\mathbf{\Gamma}}^{z,\top}\right)^{-1}\overline{\tilde{\mathbf{\Gamma}}}^{z,\top}\tilde{\mathbf{T}}^z([\tilde{f}_x^{-1}]_{\mathcal{Z}}(x)) + \left(\overline{\mathbf{\Gamma}}^z\overline{\mathbf{\Gamma}}^{z,\top}\right)^{-1}\tilde{b}_z \tag{45}$$

$$\mathbf{T}^s([f_x^{-1}]_{\mathcal{S}}(x)) = \left(\overline{\mathbf{\Gamma}}^s\overline{\mathbf{\Gamma}}^{s,\top}\right)^{-1}\overline{\tilde{\mathbf{\Gamma}}}^{s,\top}\tilde{\mathbf{T}}^s([\tilde{f}_x^{-1}]_{\mathcal{S}}(x)) + \left(\overline{\mathbf{\Gamma}}^s\overline{\mathbf{\Gamma}}^{s,\top}\right)^{-1}\tilde{b}_s. \tag{46}$$

$$\mathbf{T}^s(f_y^{-1}(y)) = \left(\overline{\mathbf{\Gamma}}^s\overline{\mathbf{\Gamma}}^{s,\top}\right)^{-1}\overline{\tilde{\mathbf{\Gamma}}}^{s,\top}\tilde{\mathbf{T}}^s(\tilde{f}_y^{-1}(y)) + \left(\overline{\mathbf{\Gamma}}^s\overline{\mathbf{\Gamma}}^{s,\top}\right)^{-1}\tilde{b}_s. \tag{47}$$

Denote $M_z := \left(\overline{\mathbf{\Gamma}}^z\overline{\mathbf{\Gamma}}^{z,\top}\right)^{-1}\overline{\tilde{\mathbf{\Gamma}}}^{z,\top}$, $M_s := \left(\overline{\mathbf{\Gamma}}^s\overline{\mathbf{\Gamma}}^{s,\top}\right)^{-1}\overline{\tilde{\mathbf{\Gamma}}}^{s,\top}$ and $a_s = \left(\overline{\mathbf{\Gamma}}^s\overline{\mathbf{\Gamma}}^{s,\top}\right)^{-1}\tilde{b}_s$, $a_z = \left(\overline{\mathbf{\Gamma}}^z\overline{\mathbf{\Gamma}}^{z,\top}\right)^{-1}\tilde{b}_z$. The left is to prove that M_z and M_s are invertible matrices. Denote $\bar{x} = f^{-1}(x)$. Applying the (Khemakhem, Kingma and Hyvärinen, 2020, Lemma 3) we have that there exists k_s points $\bar{x}^1, ..., \bar{x}^{k_s}$, $\tilde{\bar{x}}^1, ..., \tilde{\bar{x}}^{k_z}$ such that $\left((\mathbf{T}^s)_i'([f_x^{-1}]_{\mathcal{S}_i}(x_i^1)), ..., (\mathbf{T}^s)_i'([f_x^{-1}]_{\mathcal{S}_i}(x_i^{k_s}))\right)$ for each $i \in [q_s]$ and $\left((\mathbf{T}^z)_i'([f_x^{-1}]_{\mathcal{Z}_i}(\tilde{x}_i^1)), ..., (\mathbf{T}^z)_i'([f_x^{-1}]_{\mathcal{S}_i}(\tilde{x}_i^{k_z}))\right)$ for each $i \in [q_t]$ are linearly independent.

By differentiating Eq. (45) and Eq. (46) for each $\bar{x}^i$ with $i \in [q_s]$ and $\tilde{\bar{x}}^i$ with $i \in [q_z]$ respectively, we have that

$$\left(J_{\mathbf{T}^s}(\bar{x}^1), ..., J_{\mathbf{T}^s}(\bar{x}^{k_s})\right) = M_s \left(J_{\mathbf{T}^s \circ \tilde{f}_x^{-1} \circ f_x}(\bar{x}^1), ..., J_{\mathbf{T}^s \circ \tilde{f}_x^{-1} \circ f}(\bar{x}^{k_s})\right) \tag{48}$$

$$\left(J_{\mathbf{T}^z}(\tilde{\bar{x}}^1), ..., J_{\mathbf{T}^z}(\tilde{\bar{x}}^{k_z})\right) = M_z \left(J_{\mathbf{T}^z \circ \tilde{f}_x^{-1} \circ f_x}(\tilde{\bar{x}}^1), ..., J_{\mathbf{T}^z \circ \tilde{f}_x^{-1} \circ f_x}(\tilde{\bar{x}}^{k_z})\right). \tag{49}$$

The linearly independence of $\left((\mathbf{T}^s)_i'([f_x^{-1}]_{\mathcal{S}_i}(x_i^1)), ..., (\mathbf{T}^s)_i'([f_x^{-1}]_{\mathcal{S}_i}(x_i^{k_s}))\right)$ and $\left((\mathbf{T}^z)_i'([f_x^{-1}]_{\mathcal{Z}_i}(\tilde{x}_i^1)), ..., (\mathbf{T}^z)_i'([f_x^{-1}]_{\mathcal{S}_i}(\tilde{x}_i^{k_z}))\right)$ imply that the $\left(J_{\mathbf{T}^s}(\bar{x}^1), ..., J_{\mathbf{T}^s}(\bar{x}^{k_s})\right)$ and $\left(J_{\mathbf{T}^z}(\tilde{\bar{x}}^1), ..., J_{\mathbf{T}^z}(\tilde{\bar{x}}^{k_z})\right)$ are invertible, which implies the invertibility of matrix M_s and M_z. The rest is to prove $p_{f_y}(y|[f_x]_{\mathcal{S}}^{-1}(x)) = p_{\tilde{f}_y}(y|[\tilde{f}_x]_{\mathcal{S}}^{-1}(x))$. This can be shown by applying Eq. (31) again. Specifically, according to Eq. (31), we have that

$$\begin{aligned}
&\int_{\mathcal{X}} p_{\varepsilon_x}(x - \bar{x}) p(y|[f_x]_{\mathcal{S}}^{-1}(\bar{x})) p_{\mathbf{T}^s, \mathbf{\Gamma}^s, \mathbf{T}^z, \mathbf{\Gamma}^z}(f^{-1}(\bar{x})|d^e) \mathrm{vol} J_{f^{-1}}(\bar{x}) d\bar{x} \\
&\quad = \int_{\mathcal{X}} p_{\varepsilon_x}(x - \bar{x}) p(y|[\tilde{f}_x]_{\mathcal{S}}^{-1}(\bar{x})) p_{\mathbf{T}^s, \mathbf{\Gamma}^s, \mathbf{T}^z, \mathbf{\Gamma}^z}(\tilde{f}^{-1}(\bar{x})|d^e) \mathrm{vol} J_{\tilde{f}^{-1}}(\bar{x}) d\bar{x}.
\end{aligned} \tag{50}$$

Denote $l_{\mathbf{T}^s, \mathbf{\Gamma}^s, \mathbf{T}^z, \mathbf{\Gamma}^z, f_y, f_x, y}(x) := p_{f_y}(y|[f_x]_{\mathcal{S}}^{-1}(\bar{x})) p_{\mathbf{T}^s, \mathbf{\Gamma}^s, \mathbf{T}^z, \mathbf{\Gamma}^z}(f^{-1}(\bar{x})|d^e) \mathrm{vol} J_{f_x^{-1}}(\bar{x})$, we have

$$\int_{\mathcal{X}} p_{\varepsilon_x}(x - \bar{x}) l_{\mathbf{T}^s, \mathbf{\Gamma}^s, \mathbf{T}^z, \mathbf{\Gamma}^z, f_y, f_x, y}(\bar{x}) d\bar{x} = \int_{\mathcal{X}} p_{\varepsilon_x}(x - \bar{x}) l_{\tilde{\mathbf{T}}^s, \tilde{\mathbf{\Gamma}}^s, \tilde{\mathbf{T}}^z, \tilde{\mathbf{\Gamma}}^z, \tilde{f}_y, \tilde{f}_x, y}(\bar{x}) d\bar{x} \tag{51}$$

$$\Longrightarrow (l_{\mathbf{T}^s, \mathbf{\Gamma}^s, \mathbf{T}^z, \mathbf{\Gamma}^z, f_y, f_x, y} * p_{\varepsilon_x})(x|d^e) = (l_{\tilde{\mathbf{T}}^s, \tilde{\mathbf{\Gamma}}^s, \tilde{\mathbf{T}}^z, \tilde{\mathbf{\Gamma}}^z, \tilde{f}_y, \tilde{f}_x, y} * p_{\varepsilon_x})(x|d^e) \tag{52}$$

$$\Longrightarrow F[l_{\tilde{\mathbf{T}}^s, \tilde{\mathbf{\Gamma}}^s, \tilde{\mathbf{T}}^z, \tilde{\mathbf{\Gamma}}^z, \tilde{f}_y, \tilde{f}_x, y}](\omega) \varphi_{\varepsilon_x}(\omega) = F[l_{\mathbf{T}^s, \mathbf{\Gamma}^s, \mathbf{T}^z, \mathbf{\Gamma}^z, f_y, f_x, y}](\omega) \varphi_{\varepsilon_x}(\omega) \tag{53}$$

$$\Longrightarrow F[l_{\mathbf{T}^s, \mathbf{\Gamma}^s, \mathbf{T}^z, \mathbf{\Gamma}^z, f_y, f_x, y}](\omega) = F[l_{\tilde{\mathbf{T}}^s, \tilde{\mathbf{\Gamma}}^s, \tilde{\mathbf{T}}^z, \tilde{\mathbf{\Gamma}}^z, \tilde{f}_y, \tilde{f}_x, y}](\omega) \tag{54}$$

$$\Longrightarrow l_{\mathbf{T}^s, \mathbf{\Gamma}^s, \mathbf{T}^z, \mathbf{\Gamma}^z, f_y, f_x, y}(x) = l_{\tilde{\mathbf{T}}^s, \tilde{\mathbf{\Gamma}}^s, \tilde{\mathbf{T}}^z, \tilde{\mathbf{\Gamma}}^z, \tilde{f}_y, \tilde{f}_x, y}(x) \tag{55}$$

$$\begin{aligned}
\Longrightarrow & p_{f_y}(y|[f_x]_{\mathcal{S}}^{-1}(x)) p_{\mathbf{T}^s, \mathbf{\Gamma}^s, \mathbf{T}^z, \mathbf{\Gamma}^z}(f^{-1}(x)|d^e) \mathrm{vol} J_{f_x^{-1}}(x) \\
& = p_{\tilde{f}_y}(y|[\tilde{f}_x]_{\mathcal{S}}^{-1}(x)) p_{\tilde{\mathbf{T}}^s, \tilde{\mathbf{\Gamma}}^s, \tilde{\mathbf{T}}^z, \tilde{\mathbf{\Gamma}}^z}(\tilde{f}^{-1}(x)|d^e) \mathrm{vol} J_{\tilde{f}_x^{-1}}(x).
\end{aligned} \tag{56}$$

Taking the log transformation on both sides of Eq. (56), we have that

$$\begin{aligned}
&\log p_{f_y}(y|[f_x]_{\mathcal{S}}^{-1}(x)) + \log p_{\mathbf{T}^s, \mathbf{\Gamma}^s, \mathbf{T}^z, \mathbf{\Gamma}^z}(f^{-1}(x)|d^e) + \log \mathrm{vol} J_{f_x^{-1}}(x) \\
&\quad = \log p_{\tilde{f}_y}(y|[\tilde{f}_x]_{\mathcal{S}}^{-1}(x)) + \log p_{\tilde{\mathbf{T}}^s, \tilde{\mathbf{\Gamma}}^s, \tilde{\mathbf{T}}^z, \tilde{\mathbf{\Gamma}}^z}(\tilde{f}^{-1}(x)|d^e) + \log \mathrm{vol} J_{\tilde{f}_x^{-1}}(x).
\end{aligned} \tag{57}$$

Subtracting Eq. (57) with y_2 from Eq. (57) with y_1, we have

$$\frac{p_{f_y}(y_2|[f_x]_{\mathcal{S}}^{-1}(x))}{p_{f_y}(y_1|[f_x]_{\mathcal{S}}^{-1}(x))} = \frac{p_{\tilde{f}_y}(y_2|[\tilde{f}_x]_{\mathcal{S}}^{-1}(x))}{p_{\tilde{f}_y}(y_1|[\tilde{f}_x]_{\mathcal{S}}^{-1}(x))} \tag{58}$$

$$\Longrightarrow \int_{\mathcal{Y}} \frac{p_{f_y}(y_2|[f_x]_{\mathcal{S}}^{-1}(x))}{p_{f_y}(y_1|[f_x]_{\mathcal{S}}^{-1}(x))} dy_2 = \int_{\mathcal{Y}} \frac{p_{\tilde{f}_y}(y_2|[\tilde{f}_x]_{\mathcal{S}}^{-1}(x))}{p_{\tilde{f}_y}(y_1|[\tilde{f}_x]_{\mathcal{S}}^{-1}(x))} dy_2 \tag{59}$$

$$\Longrightarrow p_{f_y}(y_1|[f_x]_{\mathcal{S}}^{-1}(x)) = p_{\tilde{f}_y}(y_1|[\tilde{f}_x]_{\mathcal{S}}^{-1}(x)), \tag{60}$$

for any $y_1 \in \mathcal{Y}$. This completes the proof. □

Understanding the assumption (4) in Theorem 7.9 and 7.6. Recall that we assume the confounder d_s in LaCIM is the source variable for generating data in corresponding domain. Here we also use the $\mathcal{C}$ to denote the space of d_s (since $d_s := c$), then we have the following theoretical conclusion that the as long as the image set of $\mathcal{C}$ is not included in any sets with Lebesgue measure 0, the assumption (4) holds. This conclusion means that the assumption **(4)** holds generically.

Theorem 7.10. *Denote* $h^{t=s,z}(d) := \left(\Gamma_{1,1}^t(d) - \Gamma_{1,1}^t(d^{e_1}), ..., \Gamma_{q_t,k_t}^t(d) - \Gamma_{1,1}^t(d^{e_1})\right)^\top$, $h(\mathcal{C}) := h^s(\mathcal{S}) \oplus h^z(\mathcal{Z}) \subset \mathbb{R}^{q_z * k_z} \oplus \mathbb{R}^{q_s * k_s}$, *then assumption (4) holds if* $h(\mathcal{C})$ *is not included in any zero-measure set of* $\mathbb{R}^{q_z * k_z} \oplus \mathbb{R}^{q_s * k_s}$. *Denote* $r_s := q_s * k_s$ *and* $r_z := q_z * k_z$.

Proof. With loss of generality, we assume that $r_s \leq r_z$. Denote Q as the set of integers q such that there exists $d^{e_2}, ..., d^{q+1}$ that the $\text{rank}([h^z(d^{e_2}), ..., h^z(d^{e_{q+1}})]) = \min(q, r_z)$ and $\text{rank}([h^s(d^{e_2}), ..., h^s(d^{e_{q+1}})]) = \min(q, r_s)$. Denote $u := \max(Q)$. We discuss two possible cases for u, respectively:

- Case 1. $u < r_s \leq r_z$. Then there exists $d^{e_2}, ..., d^{e_{u+1}}$ s.t. $h^z(d^{e_2}), ..., h^z(d^{e_{u+1}})$ and $h^s(d^{e_2}), ..., h^s(d^{e_{u+1}})$ are linearly independent. Then $\forall c$, we have $h^z(d) \in L(h^z(d^{e_2}), ..., h^z(d^{e_{u+1}}))$ or $h^s(d) \in L(h^s(d^{e_2}), ..., h^s(d^{e_{u+1}}))$. Therefore, so we have $h^z(d) \oplus h^s(d) \in [L(h^z(d^{e_2}), ..., h^z(d^{e_{u+1}})) \oplus \mathbb{R}^{r_s}] \cup [\mathbb{R}^{r_z} \oplus L(h^s(d^{e_2}), ..., h^s(d^{e_{u+1}}))]$, which has measure 0 in $\mathbb{R}^{r_z} \oplus \mathbb{R}^{r_s}$.
- Case 2. $r_s \leq u < r_z$. Then there exists $d^{e_2}, ..., d^{e_{u+1}}$ s.t. $h^z(d^{e_2}), ..., h^z(d^{e_{u+1}})$ are linearly independent and $rank([h^s(d^{e_1}), ..., h^s(d^{e_u})]) = r_s$. Then $\forall c$, we have $h^z(d) \in L(h^z(d^{e_1}), ..., h^z(d^{e_{u+1}}))$, which means that $h^z(d) \oplus h^s(d) \in L(h^z(d^{e_1}), ..., h^z(d^{e_{u+1}})) \oplus \mathbb{R}^{r_s}$, which has measure 0 in $\mathbb{R}^{r_z} \oplus \mathbb{R}^{r_s}$.

The above two cases are contradict to the assumption that $h(\mathcal{C})$ is not included in any zero-measure set of $\mathbb{R}^{r_z} \oplus \mathbb{R}^{r_s}$. □

Lemma 7.11. *Consider the cases when $k_s \geq 2$. Then suppose the assumptions in theorem 7.9 are satisfied. Further assumed that*

- *The sufficient statistics $\mathbf{T}^s_{i,j}$ are twice differentiable for each $i \in [q_s]$ and $j \in [k_s]$.*
- *f_y is twice differentiable.*

Then we have M_s in theorem 7.9 is block permutation matrix.

Proof. Directly applying (Khemakhem, Kingma and Hyvärinen, 2020, Theorem 2) with $f_x, A, b, \mathbf{T}, x$ replaced by $f_y, M_s, a_s, \mathbf{T}^s, y$. □

Lemma 7.12. *Consider the cases when $k_s = 1$. Then suppose the assumptions in theorem 7.9 are satisfied. Further assumed that*

- *The sufficient statistics $\mathbf{T}^s_i$ are not monotonic for $i \in [q_s]$.*
- *g is smooth.*

Then we have M_s in theorem 7.9 is block permutation matrix.

Proof. Directly applying (Khemakhem, Kingma and Hyvärinen, 2020, Theorem 3) with $f_x, A, b, \mathbf{T}, x$ replaced by $f_y, M_s, a_s, \mathbf{T}^s, y$. □

Proof of Theorem 7.6. According to theorem 7.9, there exist invertible matrices M_s and M_z such that

$$\begin{aligned}
&\mathbf{T}(f_x^{-1}(x)) = A\tilde{\mathbf{T}}(\tilde{f}_x^{-1}(x)) + b \\
&\mathbf{T}^s([f_x^{-1}]_{\mathcal{S}}(x)) = M_s\tilde{\mathbf{T}}^s([\tilde{f}_x^{-1}]_{\mathcal{S}}(x)) + a_s. \\
&\mathbf{T}^s(f_y^{-1}(y)) = M_s\tilde{\mathbf{T}}^s(\tilde{f}_y^{-1}(y)) + a_s,
\end{aligned}$$

where $\mathbf{T} = [\mathbf{T}^{s,\top}, \mathbf{T}^{z,\top}]^\top$, and

$$A = \begin{pmatrix} M_s & 0 \\ 0 & M_z \end{pmatrix}. \tag{61}$$

By further assuming that the sufficient statistics $\mathbf{T}^s_{i,j}$ are twice differentiable for each $i \in [q_s]$ and $j \in [k_s]$ for $k_s \geq 2$ and not monotonic for $k_s = 1$. Then we have that M_s is block permutation matrix. By further assuming that $\mathbf{T}^z_{i,j}$ are twice differentiable for each $i \in [n_z]$ and $j \in [k_z]$ for $k_z \geq 2$ and not monotonic for $k_z = 1$ and applying the lemma 7.11 and 7.12 respectively, we have that A is block permutation matrix. Therefore, M_z is also a block permutation matrix. □

Proof of Theorem 4.3. We consider the general case when $\mathcal{C} := \cup_{r=1}^{R} \mathcal{C}_r$, in which each $\mathcal{C}_r$ can be simplified as a representative point c_r. For environment d^e, let $\mathrm{P}_{d^e} = [\mathrm{P}(C = c_1|d^e), \cdots, \mathrm{P}(C = c_R|d^e)]$ be the vector of probability mass of C in the environment d^e. And $\mathcal{E}_{train}$ has m environments with indexes $d^{e_1}, \cdots, d^{e_m}$. The latent factors (S, Z) belongs to the exponential family distribution $p(s, z|c) = p_{\mathbf{T}^z, \mathbf{\Gamma}^z(d)}(z) p_{\mathbf{T}^s, \mathbf{\Gamma}^s(d)}(s)$. Suppose that $\theta = \{f_x, f_y, \mathbf{T}^s, \mathbf{T}^z\}$ and $\tilde{\theta} = \{\tilde{f}_x, \tilde{g}_y, \tilde{\mathbf{T}}^s, \tilde{\mathbf{T}}^z\}$ share the same observational distribution for each environment, *i.e.*, $p_\theta(x, y|d^e) = p_{\tilde{\theta}}(x, y|d^e)$, then we have that

$$\sum_{r=1}^{R} p_\theta(x, y|c_r) \, \mathrm{P}(C = c_r|d^e) = \sum_{r=1}^{R} p_{\tilde{\theta}}(x, y|c_r) \, \mathrm{P}(C = c_R|d^e). \tag{62}$$

Let $\Delta_{x,y} = [p_\theta(x, y|c_1) - p_{\tilde{\theta}}(x, y|c_1), \cdots, p_\theta(x, y|c_m) - p_{\tilde{\theta}}(x, y|c_m)]^\mathsf{T}$, then Eq. (62) can be written as $A\Delta_{x,y} = 0$. Denote $A := \mathrm{P}_{d^{e_1}}^\top \in \mathbb{R}^{m \times R}$. According the *diversity condition*, we have that A and the $[[\mathbf{\Gamma}^t(c_2) - \mathbf{\Gamma}^t(c_1)]^\mathsf{T}, ..., [\mathbf{\Gamma}^t(c_m) - \mathbf{\Gamma}^t(c_1)]^\mathsf{T}]^\mathsf{T}$ have full column rank, therefore we have that $\Delta_{x,y} = 0$, *i.e.* $p_\theta(x, y|c_r) = p_{\tilde{\theta}}(x, y|c_r)$ for each $r \in [R]$. The left proof is the same with the one in theorem 7.6. □

7.4 Proof of Theorem 4.4

Proof of Theorem 4.4. Due to Eq. (62), it is suffices to prove the conclusion for every $c_r \in \{c_r\}_{r \in [R]}$. Motivated by Barron and Sheu (1991, Theorem 2) that the distribution $p^e(s, z)$ defined on bounded set can be approximated by a sequence of exponential family with sufficient statistics denoted as polynomial terms, therefore the $\mathbf{T}^{t=s,z}$ are twice differentiable hence satisfies the assumption (2) in theorem 4.3 and assumption (1) in lemma 7.11. Besides, the lemma 4 in Barron and Sheu (1991) informs us that the KL divergence between $p_{\theta_0}(s, z|c_r)$ ($\theta_0 := (f_x, f_y, \boldsymbol{T}^z, \boldsymbol{T}^s, \mathbf{\Gamma}_0^z, \mathbf{\Gamma}_0^s)$ and $p_{\theta_1}(s, z|c_r)$ ($\theta_1 := (f_x, f_y, \boldsymbol{T}^z, \boldsymbol{T}^s, \mathbf{\Gamma}_1^z, \mathbf{\Gamma}_1^s)$ (the $p_{\theta_0}(s, z|c_r), p_{\theta_1}(s, z|c_r)$ belong to exponential family with polynomial sufficient statistics terms) can be bounded by the ℓ_2 norm of $[(\mathbf{\Gamma}^s(c_r) - \mathbf{\Gamma}_1^s(c_r))^\top, (\mathbf{\Gamma}_0^z(c_r) - \mathbf{\Gamma}_1^z(c_r))^\top]^\top$. Therefore, $\forall \epsilon > 0$, there exists a open set of $\Gamma(c_r)$ such that the $D_{\mathrm{KL}}(p(s, z|c_r), p_\theta(s, z|c_r)) < \epsilon$. Such an open set is with non-zero Lebesgue measurement therefore can satisfy the assumption (4) in theorem 4.3, according to result in theorem 7.10. The left is to prove that for any p defined by a LaCIM following Def. 4.1, there is a sequence of $\{p_m\}_n \in \mathcal{P}_{\exp}$ such that the $d_{\mathrm{Pok}}(p, p_n) \to 0$ that is equivalent to $p_n \xrightarrow{d} p$. For any A, B, we consider to prove that

$$I_n \triangleq \Big| p(x \in A, y \in B|c_r) - p_n(x \in A, y_n \in B|c_r) \Big| \to 0, \tag{63}$$

where $p_n(x \in A, y_n \in B|c_r) = \int_{\mathcal{S}} \int_{\mathcal{Z}} p(x \in A|s, z) p(y_n \in B|s) p_n(s, z|c_r) ds dz$ with

$$y_n(i) = \frac{\exp((f_{y,i}(\boldsymbol{s}) + \varepsilon_{y,i})/T_n)}{\sum_i \exp((f_{y,i}(\boldsymbol{s}) + \varepsilon_{y,i})/T_n)}, \ i = 1, ..., k, \tag{64}$$

for $y \in \mathbb{R}^k$ denoting the k-dimensional one-hot vector for categorical variable and $\varepsilon_{y,1,...,k}$ are Gumbel i.i.d. According to (Maddison et al., 2016, Proposition 1) that the $y_n(i) \xrightarrow{d} y(i)$ with

$$p(y(i) = 1) = \frac{\exp(f_{y,i}(\boldsymbol{s}))}{\sum_i \exp((f_{y,i}(\boldsymbol{s}))}, \ as \ T_n \to 0. \tag{65}$$

As long as f_y is smooth, we have that the $p(y_n|s)$ is continuous. We have that

$$\begin{aligned}
I_n &= \Big| p(x \in A, y \in B|c_r) - \int_{\mathcal{S} \times \mathcal{Z}} p(x \in A|s, z) p(y_n \in B|s) p_n(s, z|c_r) ds dz \Big| \\
&\leq \Big| p(x \in A, y \in B|c_r) - p(x \in A, y_n \in B|c_r) \Big| \\
&\qquad + \Big| p(x \in A, y_n \in B|c_r) - \int_{\mathcal{S} \times \mathcal{Z}} p(x \in A|s, z) p(y_n \in B|s) p_n(s, z|c_r) ds dz \Big| \\
&= \Big| \int_{\mathcal{S} \times \mathcal{Z}} p(x \in A|s, z) \left(p(y \in B|s) - p(y_n \in B|s) \right) p(s, z|c_r) ds dz \Big| \\
&\qquad + \Big| \int_{\mathcal{S} \times \mathcal{Z}} p(x \in A|s, z) p(y_n \in B|s) \left(p(s, z|c_r) - p_n(s, z|c_r) \right) \Big|
\end{aligned}$$

$$
\begin{aligned}
&\leq \underbrace{\left| \int_{M_s \times M_z} p(x \in A|s,z) \left(p(y \in B|s) - p(y_n \in B|s)\right) p(s,z|c_r) ds dz \right|}_{I_{n,1}} \\
&+ \underbrace{\left| \int_{(M_s \times M_z)^{c_r}} p(x \in A|s,z) \left(p(y \in B|s) - p(y_n \in B|s)\right) p(s,z|c_r) ds dz \right|}_{I_{n,2}} \\
&+ \underbrace{\left| \int_{M_s \times M_z} p(x \in A|s,z) p(y_n \in B|s) \left(p(s,z|c_r) - p_n(s,z|c_r)\right) \right|}_{I_{n,3}} \\
&+ \underbrace{\left| \int_{(M_s \times M_z)^{c_r}} p(x \in A|s,z) p(y_n \in B|s) \left(p(s,z|c_r) - p_n(s,z|c_r)\right) \right|}_{I_{n,4}}. \qquad (66)
\end{aligned}
$$

For $I_{n,1}$, if y is itself additive model with $y = f_y(\boldsymbol{s}) + \varepsilon_y$, then we just set $y_n \overset{d}{=} y$, then we have that $I_{n,1} = 0$. Therefore, we only consider the case when y denotes the categorical variable with softmax distribution, *i.e.*, Eq. (65). $\forall c_r \in \mathcal{C} := \{c_1, ..., c_R\}$ and $\forall \epsilon > 0$, there exists $M_s^{c_r}$ and $M_z^{c_r}$ such that $p(s, z \in M_s^{c_r} \times M_z^{c_r}|c_r) \leq \epsilon$; Denote $M_s \overset{\Delta}{=} \cup_{k=1}^m M_s^{c_r}$ and $M_z \overset{\Delta}{=} \cup_{k=1}^m M_z^{c_r}$, we have that $p(s, z \in M_s \times M_z|c) \leq 2\epsilon$ for all $c_r \in \mathcal{C}$. Since $\forall s_1 \in M_s$, $\exists N_{s_1}$ such that $\forall n \geq N_{s_1}$, we have that $\Big|p(y \in B|s_1) - p(y \in B|s_1)| \leq \epsilon$ from that $y_n \overset{d}{\to} y$. Besides, there exists open set $\mathcal{O}_{s_1}$ such that $\forall s \in \mathcal{O}_{s_1}$ and

$$
\Big|p(y \in B|s_1) - p(y \in B|s_1)| \leq \epsilon, \ \Big|p(y_n \in B|s_1) - p(y_n \in B|s_1)| \leq \epsilon.
$$

Again, according to Heine–Borel theorem, there exists finite s, namely $s_1, ..., s_l$ such that $M_s \subset \cup_{i=1}^l \mathcal{O}(s_i)$. Then there exists $N \overset{\Delta}{=} \max\{N_{s_1}, ..., N_{s_l}\}$ such that $\forall n \geq N$, we have that

$$
\Big|p(y \in B|s) - p(y_n \in B|s)\Big| \leq 3\epsilon, \ \forall s \in M_s. \qquad (67)
$$

Therefore, $I_{n,1} \leq \int_{M_s \times M_z} 3\epsilon p(x \in A|s,z) p(s,z|c) ds dz \leq 3\epsilon$. Hence, $I_{n,1} \to 0$ as $n \to \infty$. Besides, we have that $I_{n,2} \leq \int_{M_s \times M_z} 2\epsilon p(s,z|c_r) ds dz \leq 2\epsilon$. Therefore, we have that $\Big| \int_{\mathcal{S} \times \mathcal{Z}} p(x \in A|s,z) \left(p(y \in B|s) - p(y_n \in B|s)\right) p(s,z|c_r) ds dz \Big| \to 0$ as $n \to \infty$. For $I_{n,3}$, we have that

$$
\begin{aligned}
I_{n,3} &= \left| \int_{M_s \times M_z} p(x \in A|s,z) p(y_n \in B|s) \mathbb{1}(s, z \in M_s \times M_z) \left(p(s,z|c_r) - p_n(s,z|c_r)\right) ds dz \right| \\
&\leq \underbrace{\left| \int_{M_s \times M_z} p(x \in A|s,z) p(y_n \in B|s) p(s,z|c_r) \left(\frac{1}{p(s, z \in M_s \times M_z|c_r)} - 1 \right) ds dz \right|}_{I_{n,3,1}} \\
&+ \underbrace{\left| \int_{M_s \times M_z} p(x \in A|s,z) p(y_n \in B|s) p(s,z|c_r) \left(\frac{1}{p(s, z \in M_s \times M_z|c_r)} - 1 \right) ds dz \right|}_{I_{n,3,2}}.
\end{aligned} \qquad (68)
$$

The $I_{n,3,1} \leq \frac{\epsilon}{1-\epsilon}$. Denote $\tilde{p}(s,z|c_r) := \frac{p(s,z|c_r)\mathbb{1}(s,z \in M_s \times M_z)}{p(s,z \in M_s \times M_z|c_r)}$, according to (Barron and Sheu, 1991, Theorem 2), there exists a sequence of $p_n(s,z|c)$ defined on a compact support $M_s \times M_z$ such that $\forall c_r \in \mathcal{C}$, we have that

$$
p_n(s,z|c_r) \overset{d}{\to} p(s,z|c_r).
$$

Applying again the Heine–Borel theorem, we have that $\forall \epsilon$, $\exists N$ such that $\forall n \geq N$, we have

$$
\Big|\tilde{p}(s,z|c_r) - p_n(s,z|c_r)\Big| \leq \epsilon, \qquad (69)
$$

which implies that $I_{n,3,2} \to 0$ as $n \to \infty$ combining with the fact that $p(x, y|s, z)$ is continuous with respect to s, z. For $I_{n,4}$, we have that

$$I_{n,4} = \left| \int_{M_s \times M_z} p(x \in A|s, z)p(y_n \in B|s)p(s, z|c_r) \right| \leq \left| \int_{M_s \times M_z} p(s, z|c_r) \right| \leq \epsilon, \tag{70}$$

where the first equality is from that the $p_n(s, z|c_r)$ is defined on $M_s \times M_z$. Then we have that

$$\left| \int_{\mathcal{S} \times \mathcal{Z}} p(x \in A|s, z)p(y_n \in B|s) \left(p(s, z|c_r) - p_n(s, z|c)\right) \right| \to 0, \ as \ n \to \infty. \tag{71}$$

The proof is completed. □

7.5 Reparameterization for LaCIM-d

We provide an alternative training method to avoid parameterization of prior $p(s, z|d^e)$ to increase the diversity of generative models in different environments. Specifically, motivated by Hyvärinen and Pajunen (1999) that any distribution can be transformed to isotropic Gaussian with the density denoted by p_{Gau}, we have that for any $e \in \mathcal{E}_{\text{train}}$, we have

$$\begin{aligned} p^e(x, y) &= \int_{\mathcal{S} \times \mathcal{Z}} p_{f_x}(x|s, z)p_{f_y}(y|s)p(s, z|d^e)dsdz \\ &= \int_{\mathcal{S} \times \mathcal{Z}} p(x|(\rho_s^e)^{-1}(s'), (\rho_z^e)^{-1}(z'))p(y|\rho_s(s'))p_{\text{Gau}}(s', z')ds'dz', \end{aligned}$$

with $s', z' := \rho_s^e(s), \rho_z^e(z) \sim \mathcal{N}(0, I)$. We can then rewrite ELBO for LaCIM-d for environment e as:

$$\begin{aligned} \mathcal{L}^e_{\phi,\psi,\rho^e} &= \mathbb{E}_{p^e(x,y)} \left[-\log q_\psi^e(y|x) \right] \\ &\quad + \mathbb{E}_{p^e(x,y)} \left[-\mathbb{E}_{q_\psi^e(s,z|x)} \frac{q_\psi(y|(\rho_s^e)^{-1}(s))}{q_\psi^e(y|x)} \log \frac{p_\phi((\rho_s^e)^{-1}(s), (\rho_z^e)^{-1}(z))p_{\text{Gau}}(s, z)}{q_\psi^e(s, z|x)} \right]. \end{aligned} \tag{72}$$

7.6 Identifiability

Earlier works that identify the latent confounders rely on strong assumptions regarding the causal structure, such as the linear model from latent to observed variable or ICA in which the latent component are independent Silva et al. (2006), or noise-free model Shimizu et al. (2009); Davies (2004). The Hoyer et al. (2008); Janzing, Peters, Mooij and Schölkopf (2012) extend to the additive noise model (ANM) and other causal discovery assumptions. Although the Lee et al. (2019) relaxed the constraints put on the causal structure, it required the latent noise is with small strength, which does not match with many realistic scenarios, such as the structural MRI of Alzheimer's Disease considered in our experiment. The works which also based on the independent component analysis (ICA), *i.e.*, the latent variables are (conditionally) independent, include Davies (2004); Eriksson and Koivunen (2003); recently, a series of works extend the above results to deep nonlinear ICA (Hyvarinen and Morioka, 2016; Hyvärinen et al., 2019; Khemakhem, Kingma and Hyvärinen, 2020; Khemakhem, Monti, Kingma and Hyvärinen, 2020; Teshima et al., 2020). However, these works require that the value of confounder of these latent variables is fixed, which cannot explain the spurious correlation in a single dataset. In contrast, our result can incorporate these scenarios by assuming that each sample has a specific value of the confounder. Other works assume discrete distribution for latent variables, such as Janzing, Sgouritsa, Stegle, Peters and Schölkopf (2012); Kocaoglu et al. (2018); Sgouritsa et al. (2013). However, in the literature, no existing works can disentangle the prediction-causative features from others, in the scenario of avoiding spurious correlation in order for OOD generalization.

7.7 Comparison with existing works

7.7.1 $Y \to S$ or $S \to Y$?

Many existing works Rojas-Carulla et al. (2018); Khemakhem, Monti, Kingma and Hyvärinen (2020); Ilse et al. (2020; 2019) assumed $Y \to S(X)$ as the causal direction. Such an difference from ours

can mainly be contributed to the generating process of Y. Different understanding leads to different causal graph. The example of digital hand-writing in Peters et al. (2017) provides a good explanation. Consider the case that the writer is provided with a label first (such as "2") before writing the digit (denoted as X), then it should be $Y \to X$. Consider another case, when the writing is based on the incentive (denoted as S) of which digit to write, then the writer record the label Y and the digit X concurrently, in which case it should be $X \leftarrow S \to Y$. For $Y \to S$, the Y is thought to be the source variable that generates the latent components and is observed before X. In contrast, we define Y as ground-truth labels given by humans. Taking image classification as an example, it is the human that give the classification of all things such as animals. In this case, it can be assumed that the label given by humans are ground-truth labels. This assumption can be based by the work Biederman (1987) in the field of psychology that humans can factorize the image X by many components due to the powerful perception learning ability of human beings. These components which denoted as S, can be accurately detected by humans, therefore we can approximately assume that it is the S generating the label Y. Consider the task of early prediction in Alzheimer's Disease, the disease label is given based on the pathological analysis and observed after the MRI X. Such a labelling outcome can be regarded as the ground-truth which itself is defined by medical science. The corresponding pathology features, as the evidences for labelling, can also thought as the generators of X. In these cases, it is more appropriate to assume the Y as the outcome than the cause. For example, the Peters et al. (2016); Kuang et al. (2018) assumed $X_S \to Y$. As an adaptation to sensory-level data such as image, we assume $S \to Y$ with S are latent variables to model high-level explanatory factors, which coincides with existing literature Teshima et al. (2020). Another difference lies in the definition of Y. The Invariant Risk Minimization (we will give a detailed comparison later) Arjovsky et al. (2019) assumes that $X \to \tilde{S} \to Y$ by defining the Y as the label with noise. The $\tilde{S}$ denoted as the extracted hidden components by observer.

7.7.2 Comparisons with data augmentation & architecture design

The goal of data augmentation Shorten and Khoshgoftaar (2019) is increase the variety of the data distribution, such as geometrical transformation Kang et al. (2017); Taylor and Nitschke (2017), flipping, style transfer Gatys et al. (2015), adversarial robustness Madry et al. (2017). On the other way round, an alternative kind of approaches is to integrate into the model corresponding modules that improve the robustness to some types of variations, such as Worrall et al. (2017); Marcos et al. (2016).

However, these techniques can only make effect because they are included in the training data for neural network to memorize Zhang et al. (2016); besides, the improvement is only limited to some specific types of variation considered. As analyzed in Xie et al. (2020); Krueger et al. (2020), the data augmentation trained with empirical risk minimization or robust optimization Ben-Tal et al. (2009) such as adversarial training Madry et al. (2017); Sagawa et al. (2019) can only achieve robustness on interpolation (convex hull) rather than extrapolation of training environments.

7.7.3 Comparisons with existing works in domain adaptation

Apparently, the main difference lies in the problem setting that (i) the domain adaptation (DA) can access the input data of the target domain while ours cannot; and (ii) our methods need multiple training data while the DA only needs one source domain. For methodology, our LaCIM shares insights but different with DA. Specifically, both methods assume some types of invariance that relates the training domains to the target domain. For DA, one stream is to assume the same conditional distribution shared between the source and the target domain, such as covariate shift Huang et al. (2007); Ben-David et al. (2007); Johansson et al. (2019); Sugiyama et al. (2008) in which $P(Y|X)$ are assumed to be the same across domains, concept shift Zhang et al. (2013) in which the $P(X|Y)$ is assumed to be invariant. Such an invariance is related to representation, such as $\Phi(X)$ in Zhao et al. (2019) and $P(Y|\Phi(X))$ in Pan et al. (2010); Ganin et al. (2016); Magliacane et al. (2018).

However, these assumptions are only distribution-level rather than the underlying causation which takes the data-generating process into account. Taking the image classification again as an example, our method first propose a causal graph in which the latent factors are introduced as the explanatory/causal factors of the observed variables. These are supported by the framework of generative model Khemakhem, Kingma and Hyvärinen (2020); Khemakhem, Monti, Kingma and Hyvärinen (2020); Kingma and Welling (2014); Suter et al. (2019) which has natural connection with the causal

graph Schölkopf (2019) that the edge in the causal graph reflects both the causal effect and also the generating process. Until now, perhaps the most similar work to us are Romeijn and Williamson (2018) and Teshima et al. (2020) which also need multiple training domains and get access to a few samples in the target domain. Both work assumes the similar causal graph with us but unlike our LaCIM, they do not separate the latent factors which can not explain the spurious correlation learned by supervised learning Ilse et al. (2020). Besides, the multiple training datasets in Romeijn and Williamson (2018) refer to intervened data which may hard to obtain in some applications. We have verified in our experiments that explicitly disentangle the latent variables into two parts can result in better OOD prediction power than mixing them together.

7.7.4 Comparisons with domain generalization

For domain generalization (DG), similar to the invariance assumption in DA, a series of work proposed to align the representation $\Phi(X)$ that assumed to be invariant across domains Li et al. (2017; 2018); Muandet et al. (2013). As discussed above, these methods lack the deep delving of the underlying causal structure and precludes the variations of unseen domains.

Recently, a series of works leverage causal invariance to enable OOD generalization on unseen domains, such as Ilse et al. (2019) which learns the representation that is domain-invariant. Notably, the Invariant Causal Prediction Peters et al. (2016) formulates the assumption in the definition of Structural Causal Model and assumes that $Y = X_{\mathcal{S}}\beta^{\star}_{\mathcal{S}} + \varepsilon_Y$ where ε_Y satisfies Gaussian distribution and $\mathcal{S}$ denotes the subset of covariates of X. The Rojas-Carulla et al. (2018); Bühlmann (2018) relaxes such an assumption by assuming the invariance of f_y and noise distribution ε_y in $Y \leftarrow f_y(X_{\mathcal{S}}, \varepsilon_y)$ which induces $P(Y|X_{\mathcal{S}})$. The similar assumption is also adopted in Kuang et al. (2018). However, these works causally related the output to the observed input, which may not hold in many real applications in which the observed data is sensory-level, such as audio waves and pixels. It has been discussed in Bengio et al. (2013); Bengio (2017) that the causal factors should be high-level abstractions/concepts. The Heinze-Deml and Meinshausen (2017) considers the style transfer setting in which each image is linear combination of shape-related variable and contextual-related variable, which respectively correspond to S and Z in our LaCIM in which the nonlinear mechanism (rather than linear combination in Heinze-Deml and Meinshausen (2017)) is allowed. Besides, during testing, our method can generalize to the OOD sample with intervention such as adversarial noise and contextual intervention.

Recently, the most notable work is Invariant Risk Minimization Arjovsky et al. (2019), which will be discussed in detail in the subsequent section.

7.7.5 Comparisons with Invariant Risk Minimization Arjovsky et al. (2019) and references there in

The Invariant Risk Minimization (IRM) Arjovsky et al. (2019) assumes the existence of invariant representation $\Phi(X)$ that induces the optimal classifier for all domains, *i.e.*, the $\mathbb{E}[Y|Pa(Y)]$ is domain-independent in the formulation of SCM. Similar to our LaCIM, the $Pa(Y)$ can refer to latent variables. Besides, to identify the invariance and the optimal classifier, the training environments also need to be diverse enough. As aforementioned, this assumption is almost necessary to differentiate the invariance mechanism from the variant ones. To learn such an invariance, a regularization function is proposed.

The difference of our LaCIM with IRM lies in two aspects: the direction of causal relation and the methodology. For the direction, as aforementioned in section 7.7.1, the IRM assumes $X \rightarrow S$ rather than the $S, Z \rightarrow X$ in our LaCIM. This is because the IRM defines Y as label with noise while ours definie the Y as the ground-truth label hence should be generated by the ground-truth hidden components that generating S. Such an inconsistency can be reflected by experiment regarding to the CMNIST in which the number is the causal factors of the label Y, rather than only invariant correlation. Besides, in terms of methodology, the theoretical claim of IRM only holds in linear case; in contrast, the CIMe f_x, f_y are allowed to be nonlinear.

Some other works share the similar spirit with or based on IRM. The Risk-Extrapolation (REx) Krueger et al. (2020) proposed to enforce the similar behavior of m classifiers with variance of which proposed as the regularization function. The work in Xie et al. (2020) proposed a Quasi-distribution framework that can incorporate empirical risk minimization, robust optimization and

REx. It can be concluded that the robust optimization only generalizes the convex hull of training environments (defined as interpolation) and the REx can generalize extrapolated combinations of training environments. This work lacks model of underlying causal structure, although it performs similarly to IRM experimentally. Besides, the Teney et al. (2020) proposed to unpool the training data into several domains with different environment and leverages Arjovsky et al. (2019) to learn invariant information for classifier. Recently, the Bellot and van der Schaar (2020) also assumes the invariance to be generating mechanisms and can generalize the capability of IRM when unobserved confounder exist. However, this work also lacks the analysis of identifiability result.

We finish this section with the following summary of methods in section 7.7.4 and the IRM, in terms of causal factor, invariance type, direction of causal relation, theoretical judgement and the ability to generalize to intervened data.

Table 4: Our LaCIM with related works.

	Causal Factor	Direction	Invariance Type	Theoretical Judgement	Intervention
Peters et al. (2016)	Subset of covariates X	$X_S \to Y$	Linear model with Gaussian noise	Identifiability	Yes
Rojas-Carulla et al. (2018)	Subset of covariates X	$X_S \to Y$	Linear Model	-	-
Kuang et al. (2018)	Subset of covariates X	$X_S \to Y$	Nonlinear	Confounder Balancing	-
Bühlmann (2018)	Subset of covariates X	$X_S \to Y$	Nonlinear	Identifiability	-
Arjovsky et al. (2019)	Latent variables S	$X \to S \to Y$	Linear	Identifiability	-
LaCIM (**Ours**)	Latent variables S, Z	$S, Z \to X, S \to Y$	Nonlinear	Identifiability	Yes

7.8 Implementation Details and More Results for Simulation

Data Generation We set $m = 5, n_e = 1000$ for each e. The generating process of $d_s \in \mathbb{R}^{q_{d_s}}$, $Z \in \mathbb{R}^{q_z}$, $S \in \mathbb{R}^{q_s}$, $X \in \mathbb{R}^{q_x}$ and $Y \in \mathbb{R}^{q_y}$ is introduced in the supplement 7.8. We set $q_{d_s} = q_s = q_z = q_y = 2$ and $q_x = 4$. For each environment $e \in [m]$ with $m = 5$, we generate 1000 samples $\mathcal{D}^e = \{x_i, y_i\} \overset{i.i.d}{\sim} \int p_{f_x}(x|s,z)p_{f_y}(y|s)p^e(s,z|d_s^e)dsdz$. The $d_s^e = \left(\mathcal{N}(0, I_{q_{d_s} \times q_{d_s}}) + 5 * e\right) * 2$; the $s, z|d_s^e \sim \mathcal{N}\left(\mu_{\phi^\star_{s,z}}(s,z|d_s^e), \sigma^2_{\phi^\star_{s,z}}(s,z|d_s^e)\right)$ with $\mu_{\phi^\star_{s,z}} = A^{\mu}_{s,z} * d_s^e$ and $\log \sigma_{\phi^\star_{s,z}} = A^{\sigma}_{s,z} * d_s^e$ ($A^{\mu}_{s,z}$, $A^{\sigma}_{s,z}$ are random matrices); the $x|s,z \sim \mathcal{N}\left(\mu_{\phi^\star_x}(x|s,z), \sigma^2_{\phi^\star_x}(x|s,z)\right)$ with $\mu_{\phi^\star_{s,z}} = h(A^{\mu,3}_x * h(A^{\mu,2}_x * h(A^{\mu,2}_x * [s^\top, z^\top]^\top])))$ and $\log \sigma_{\phi^\star_{s,z}} = h(A^{\sigma,3}_x * h(A^{\sigma,2}_x * h(A^{\sigma,2}_x * [s^\top, z^\top]^\top])))$ (h is LeakyReLU activation function with slope $= 0.5$ and $A^{\mu,i=1,2,3}_x$,$A^{\sigma,i=1,2,3}_x$ are random matrices); the $y|s$ is similarly to $x|s,z$ with $A^{\mu,i=1,2,3}_x$,$A^{\sigma,i=1,2,3}_x$ respectively replaced by $A^{\mu,i=1,2,3}_y$,$A^{\sigma,i=1,2,3}_y$.

Implementation Details We parameterize $p_\theta(s,z|d)$, $q_\phi(s,z|x,y,d)$, $p_\theta(x|s,z)$ and $p_\theta(y|s)$ as 3-layer MLP with the LeakyReLU activation function. The Adam with learning rate 5×10^{-4} is implemented for optimization. We set the batch size as 512 and run for 2,000 iterations in each trial.

Visualization. As shown from the visualization of S is shown in Fig. 7.8, our LaCIM can identify the causal factor S.

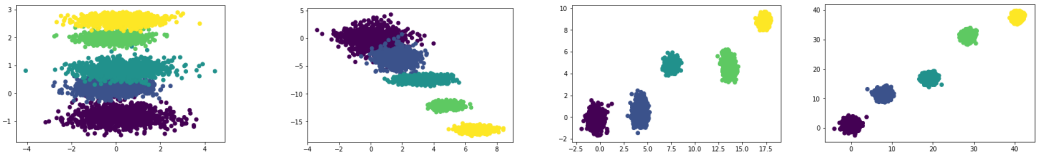

(a) $p_{\text{pool-LaCIM}}(s|x,y)$ (b) $p_{\text{LaCIM}}(s|x,y,d_s)$ (c) $p_{\text{LaCIM}}(s|x,y,d_s)$ (d) $p_{\phi^\star}(s|d_s)$

Figure 4: Visualization of S. From left to right are: estimated posterior by pool-LaCIM: $p_{\text{pool-LaCIM}}(s|x,y)$, by LaCIM with c as input: $p_{\text{LaCIM}}(s|x,y,d_s)$, by LaCIM with D as input: $p_{\text{LaCIM}}(s|x,y,d)$; the ground-truth $p_{\phi^\star}(s|d_s)$.

The setting when C can take a value in a sample-level. We consider the generation process of $\mathcal{D}^e$ as $\mathcal{D}^e = \{x_i, y_i\} \overset{i.i.d}{\sim} \int p_{f_x}(x|s,z)p_{f_y}(y|s)p(s,z|c)p(c|d^e)dsdzdc$, with $q_c := 2$. The generation is the same except that the after obtaining d_s, we additionally generate c with $c := \mathcal{N}(d_s, I)$. The results are summarized in Tab. 7.8.

Table 5: MCC of identified latent variables for $p^e(x,y) = \int p(x|s,z)p(y|s)p(s,z|c)p(c|d^e)dcdsdz$. Average over 20 times for each data.

	Data #1		Data #2		Data #3		Data #4		Data #5		Average	
	Z	S	Z	S	Z	S	Z	S	Z	S	Z	S
pool-LaCIM	0.26	0.61	0.26	0.67	0.44	0.70	0.51	0.78	0.58	0.77	0.41	0.71
LaCIM-d_s (**Ours**, $m=3$)	0.70	0.79	0.72	0.79	0.69	0.74	0.74	0.85	0.64	0.88	0.70	0.81
LaCIM-d_s (**Ours**, $m=5$)	0.73	0.85	0.70	0.89	**0.85**	0.91	0.81	0.84	**0.83**	**0.93**	0.78 ↑	0.89 ↑
LaCIM-d_s (**Ours**, $m=7$)	**0.92**	**0.90**	**0.83**	**0.90**	0.84	**0.93**	**0.85**	**0.94**	**0.83**	0.90	**0.86** ↑	**0.91** ↑

7.9 Implementation Details for Optimization over S, Z

Recall that we first optimize s^*, z^* according to

$$s^*, z^* = \arg\max_{s,z} \log p_\phi(x|s,z).$$

We first sample some initial points from each posterior distribution $q^e_\psi(s|x)$ and then optimize for 50 iterations. We using Adam as optimizer, with learning rate as 0.002 and weight decay 0.0002. The Fig. 7.9 shows the optimization effect of one run in CMNIST. As shown, the test accuracy keeps growing as iterates. For time saving, we chose to optimize for 50 iterations.

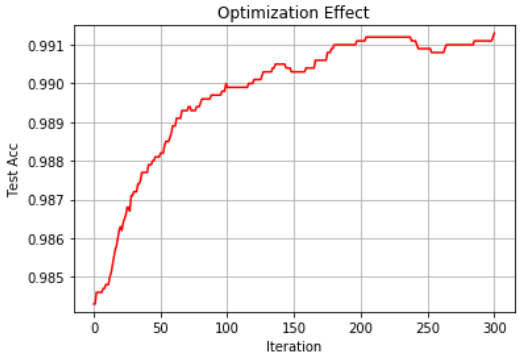

Figure 5: The optimization effect in CMNIST, starting from the point with initial sampling from inference model q of each branch. As shown, the test accuracy increases as iterates.

7.10 Implementations For Baseline

For the CE $X \to Y$ and the CE $X, d_s \to Y$, they both composed of two parts: (i) feature extractor, followed by (ii) classifier. The network structure of the feature extractor for CE $X \to Y$ is the same with that of our encoder; while the extracted features for CE $X, d \to Y$ is the concatenation of the features encoded from $X \to S, Z$ via the network with the same network structure of our encoder; and the network with the same structure of our prior network for LaCIM-d. The network structures of the classifier for both methods are the same to that of our $p_\phi(y|s)$. The IRM and SDA adopt the same structure as CE $X \to Y$. DANN adopt the same structure of CE $X \to Y$ and a additional domain classifier which is the same as that of $p_\phi(y|s)$. sVAE adopt the same structure as LaCIM-d_s with the exception that the $p_\phi(y|s)$ is replaced by $p_\phi(y|z,s)$. MMD-AAE adopt the same structure of encoder, decoder and classifier as LaCIM-d and a additional 2-layer MLP with channel 256-256-dim_z is used to extract latent z. The detailed number of parameters and channel size on each dataset for each method are summarized in Tab. 13, 14.

7.11 Supplementary for Colored MNIST

Implementation details The network structure for inference model is composed of two parts, with the first part shared among all environments and multiple branches corresponding to each environment

for the second part. The network structure of the first-part encoder is composed of four blocks, each block is the sequential of Convolutional Layer (Conv), Batch Normalization (BN), ReLU and max-pooling with stride 2. The output number of feature map is accordingly 32, 64, 128, 256. The second part network structure that output the mean and log-variance of S, Z is Conv-bn-ReLU(256) $\rightarrow$ Adaptive (1) $\rightarrow$ FC(256, 256) $\rightarrow$ ReLU $\rightarrow$ FC(256, $q_{t=s,z}$) with FC stands for fully-connected layer. The structure of $\rho_{t=s,z}$ in Eq. (72) is FC(q_t, 256) $\rightarrow$ ReLU $\rightarrow$ FC(256, q_t). The network structure for generative model $p_\phi(x|s,z)$ is the sequential of three modules: (i) Upsampling with stride 2; (ii) four blocks of Transpose-Convolution (TConv), BN and ReLU with respective output dimension being 128, 64, 32, 16; (iii) Conv-BN-ReLU-Sigmoid with number of channels in the output as 3, followed by cropping step in order to make the image with the same size as input dimension, *i.e.*, $3 \times 28 \times 28$. The network structure for generative model $p_\phi(y|s)$ is commposed of FC (512) $\rightarrow$ BN $\rightarrow$ ReLU $\rightarrow$ FC (256) $\rightarrow$ BN $\rightarrow$ ReLU $\rightarrow$ FC ($|\mathcal{Y}|$). The $q_{t=s,z}$ is set to 32. We implement SGD as optimizer with learning rate 0.5, weight decay $1e-5$ and we set batch size as 256. The total training epoch is 80.

We first explain why we do not flip y with 25% in the manuscript, and then provide further exploration of our method for the setting with flipping y.

Invariant *Causation* v.s. Invariant *Correlation* by Flipping y in Arjovsky et al. (2019) The y is further flipped with 25% to obtain the final label in IRM setting and this step is omitted in ours. The difference lies in the definition of invariance. Our LaCIM defines invariance as the causal relation between S and the label Y, while the one in IRM can be correlation. As illustrated in Handwritting Sample Form in Fig. 7.11 in Grother (1995), the generting direction should be $Y \rightarrow X$. If we denote the variable by flipping Y as $\tilde{Y}$ (*a.k.a*, the final label in IRM), then the causal graph should be $X \leftarrow Y \rightarrow \tilde{Y}$. In this case, the $\tilde{Y}$ is correlated rather than causally related to the digit X. For our LaCIM, we define the label as interpretable human label (which can approximate to y for any image x) and represented by Y in our experiments. The reason why we do not define the Y as ground-truth label is that (i) the prediction is only based on the extracted components of image which may be determined not only by the ground-truth label; (ii) the learning of ground-truth is interpretable that relevant to human. For example, if a writer is provided with digit "2" but he wrote it mistakenly as "4", then it is more interpretable that we can predict the digit as "4" rather than "2". For the digit with ambiguous label from the perspective of image, even if we predict it mistakenly, it is also interpretable in terms of prediction given the information of only digit. Returning back to the IRM setting, the label is flipping without reference to the semantic shape of digit. Therefore, the flipping may happen to noiseless digits rather than noisy and unsure ones, making the shape of number less semantically related to the label.

Experiment with IRM setting We further conduct the experiment on IRM setting, with the final label y defined by flipping original label with 25%, and further color p^e proportions of digits with corresponding color-label mapping. If we assume the original ground-truth label to be the effect of the digit number of S, then the anti-causal relation with Z and Y can make the identifiability of S difficult in this flipping scenario. Note that the causal effect between S and Y is invariant across domains, therefore we adopt to regularize the branch of inferring S to be shared among inference models for multiple environments. Besides, we regularize the causal effect between S and Z to be shared among different environments via pairwise regularization. The combined loss is formulated as:

$$\tilde{\mathcal{L}}_{\psi,\phi} = \mathcal{L}_{\psi,\phi} + \frac{\Gamma}{2m^2}\sum_{i=1}^{m}\sum_{j=1}^{m}\|\mathbb{E}_{(x,y)\sim p^{e_i}(x,y)}[y|x] - \mathbb{E}_{(x,y)\sim p^{e_j}(x,y)}[y|x]\|_2^2,$$

with $q_\psi^e(s,z|x)$ in Eq. (72) factorized as $q_{\psi_z^e}(z)q_{\psi_s}(s)$ and ρ_s shared among m environments. The appended loss is coincide with recent study Risk-Extropolation (REx) in Krueger et al. (2020), with the difference of separating y-causative factors S from others. We name such a training method as LaCIM-REx. For implementation details, in addition to shared encoder regarding S, we set learning rate as 0.1, weight decay as 0.0002, batch size as 256. we have that $p(y|x) = \int_{\mathcal{S}} q_{\psi_s}(s|x)p_\phi(y|\rho_s(s))$ for any x. We consider two settings: setting#1 with $m2$ and $p^{e_1} = 0.9, p^{e_2} = 0.8$; and setting#2 with $m = 4$ with $p^{e_1} = 0.9, p^{e_2} = 0.8, p^{e_3} = 0.7, p^{e_4} = 0.6$. We only report the number of IRM since the cross entropy performs poorly in both settings. As shown, our model performs comparably with LaCIM-d_s and better than IRM Arjovsky et al. (2019) due to separation of S znd Z.

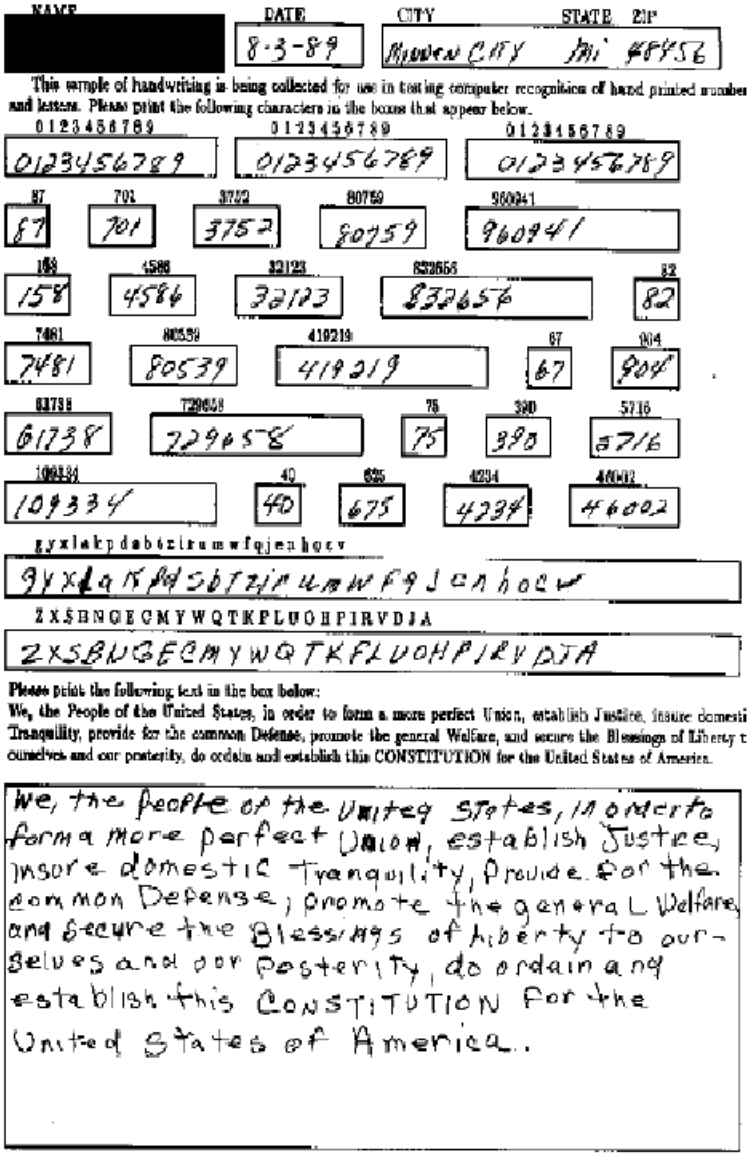

Figure 6: Hand-writting Sample Form. The writer print the digit/character (*i.e.*, X) with the label (*i.e.*, Y) provided first.

Table 6: Accuracy (%) of Colored MNIST on IRM setting in Arjovsky et al. (2019). Average over three runs.

	IRM	LaCIM-d_s (**Ours**)	LaCIM-REx (**Ours**)
$m = 2$	67.15 ± 3.79	$\mathbf{68.16 \pm 2.13}$	67.57 ± 1.37
$m = 4$	69.37 ± 1.14	$\mathbf{69.55 \pm 1.60}$	69.50 ± 0.57

7.12 SUPPLEMENTARY FOR NICO

Implementation Details Due to size difference among images, we resize each image into 256×256. The network structure of $p_\theta(z, s|d_s), q_\phi(z, s|x, d_s), p_\theta(x|z, s), p_\theta(y|s)$ for cat/dog classification is the same with the one implemented in early prediction of Alzheimer's Disease with exception of 3D convolution/Deconvolution replaced by 2D ones. For each model, we train for 200 epochs using sgd, with learning rate (lr) set to 0.01, and after every 60 epochs the learning rate is multiplied by lr decay parameter that is set to 0.2. The weight decay coefficients parameter is set to 5×10^{-4}. The

Table 7: Training and test environments (characterized by d_s)

	cat% on grass	dog% on grass	cat% on snow	cat% on snow
	Training Environment			
Env#1 ($d_s^{e_1}$)	0.6	0.4	0.1	0.9
Env#2 ($d_s^{e_2}$)	0.8	0.2	0.1	0.9
Env#3 ($d_s^{e_3}$)	0.5	0.5	0.2	0.8
Env#4 ($d_s^{e_4}$)	0.8	0.2	0.2	0.8
Env#5 ($d_s^{e_5}$)	0.7	0.3	0.2	0.8
Env#6 ($d_s^{e_6}$)	0.8	0.2	0.3	0.7
Env#7 ($d_s^{e_7}$)	0.7	0.3	0.3	0.7
Env#8 ($d_s^{e_8}$)	0.9	0.1	0.3	0.7
Env#9 ($d_s^{e_9}$)	0.4	0.6	0.3	0.7
Env#10 ($d_s^{e_{10}}$)	0.6	0.4	0.3	0.7
Env#11 ($d_s^{e_{11}}$)	0.5	0.5	0.4	0.6
Env#12 ($d_s^{e_{12}}$)	0.4	0.6	0.4	0.6
Env#13 ($d_s^{e_{13}}$)	0.7	0.3	0.4	0.6
Env#14 ($d_s^{e_{14}}$)	0.8	0.2	0.4	0.6
	Testing Environment			
Env Test d_s^{test}	0.2	0.8	0.8	0.2

Table 8: Comparison on constructed interventional dataset in terms of ACC.

Method	CE $X \to Y$	IRM	DANN	NCBB	MMD-AAE	DIVA	LaCIM-d
ACC	52.50	50.00	49.17	49.17	49.17	50.00	55.00

batch size is set to 30. The training environments which is characterized by c can be referenced in Table 7.12. For visualization, we implemented the gradient-based method Simonyan et al. (2013) to visualize the neuron (in fully connected layer for both CE $x \to y$ and CE $(x, d_s) \to y$; in s layer for LaCIM-d_s) that is most correlated to label y.

The d_s for m environments We summarize the d_s of $m = 8$ and $m = 14$ environments in Table 7.12. As shown, the value of d_s in the test domain is the extrapolation of the training environments, *i.e.*, the d_s^{test} is not included in the convex hull of $\{d^{e_i}\}_{i=1}^{14}$.

More Visualization Results Fig. 7 shows more visualization results.

Results on Intervened Data. We test our model and the baseline on intervened data, in which each image is generated by intervention on Z, i.e., taking a specific value of Z. This intervention breaks the correlation between S and Z, thus the distribution of which can be regarded as a specific type of OOD. Specifically, we replace the scene of an image with the scene from the another image, as shown in Fig. 8. We generate 120 images, including 30 images of types: cat on grass, dog on grass, cat on snow, and dog on grass. We evaluate LaCIM-d, CE $X \to Y$, IRM, DANN, NCBB, MMD-AAE, and DIVA methods on this intervened dataset. As shown in Tab 9, our LaCIM-d can performs the best among all methods, which validate the robustness of our LaCIM.

7.13 Disease Prediction of Alzheimer's Disease

Dataset Description. The dataset contains in total 317 samples with 48 AD, 75 NC, and 194 MCI.

Denotation of Attributes d_s. The $C \in \mathbb{R}^9$ includes personal attributes (*e.g.*, age Guerreiro and Bras (2015), gender Vina and Lloret (2010) and education years Mortimer (1997) that play as potential

Table 9: Comparison on constructed interventional dataset in terms of ACC.

Method	CE $X \to Y$	IRM	DANN	NCBB	MMD-AAE	DIVA	LaCIM-d
ACC	52.50	50.00	49.17	49.17	49.17	50.00	55.00

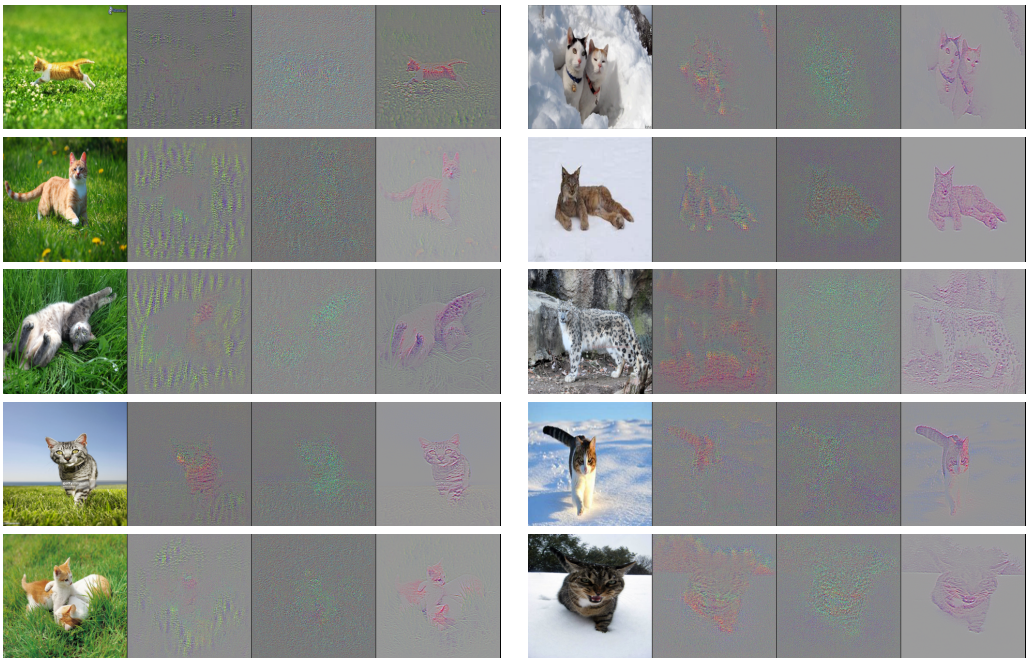

(a) Cat on grass (b) Cat on snow

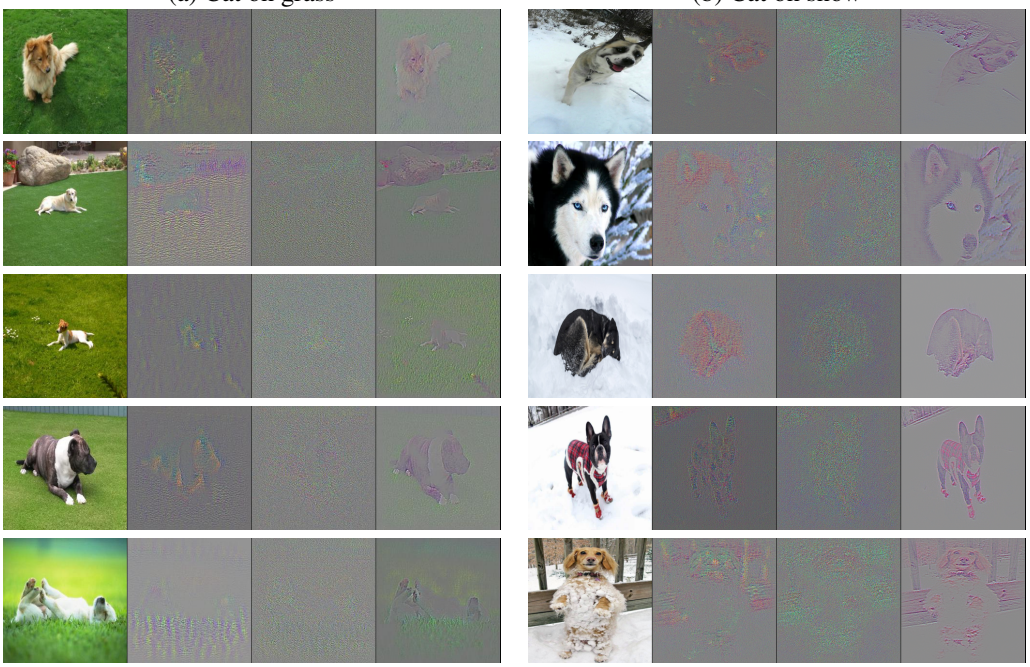

(c) Dog on grass (d) Dog on snow

Figure 7: Visualization on the NICO via gradient-based method Simonyan et al. (2013) for CE $X \to Y$, CE $(X, d_s) \to Y$ and LaCIM. The selected images are (a) cat on grass, (b) cat on snow, (c) dog on grass and (d) dog on snow.

risks of AD), gene (ε_4 allele), and biomarkers (*e.g.*, changes of CSF, TAU, PTAU, amyloid$_\beta$, cortical amyloid deposition (AV45) Humpel and Hochstrasser (2011)).

Implementation Details For LaCIM-d_s, we parameterize inference model $q_\psi(s, z|x, d_s)$, $p_\phi(s, z|d_s)$, $p_\phi(x|z, s)$ and $p_\phi(y|s)$ and $S, Z \in \mathbb{R}^{64}$. For $q_\psi(s, z|x, d_s)$, we concatenate outputs of feature extractors of X and d_s: the feature extractor for x is composed of four Convolution-Batch

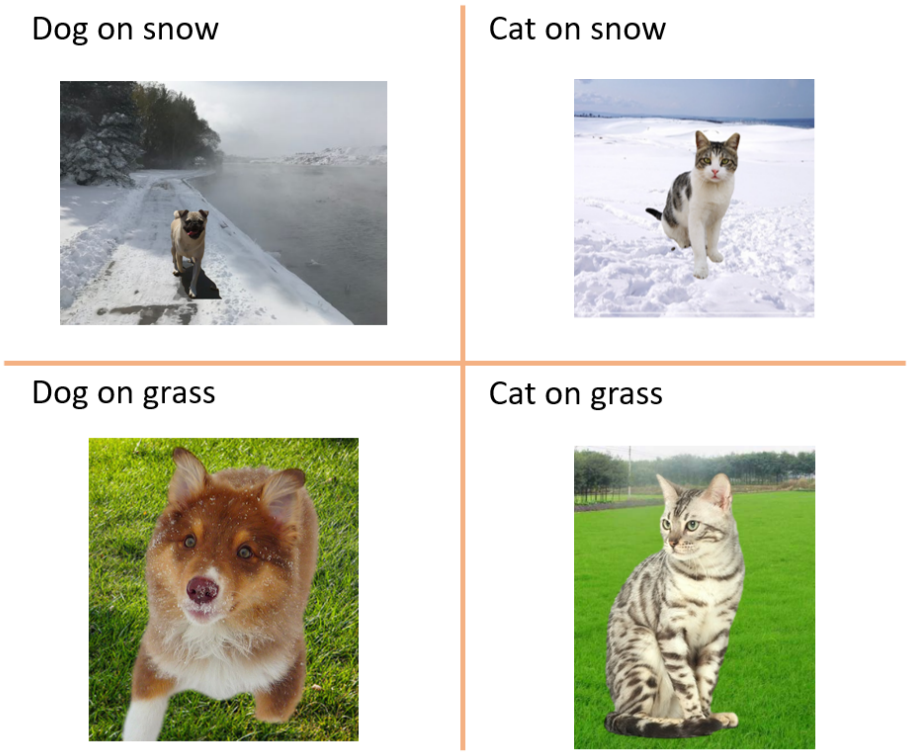

Figure 8: The constructed interventional dataset which includes of dog on snow, dog on grass, cat on snow, and dog on grass.

Normalization-ReLU (CBNR) blocks and four Convolution-Batch Normalization-ReLU-MaxPooling (CBNR-MP) blocks with structure 64 BNR $\rightarrow$ 128 CBNR-MP $\rightarrow$ 128 CBNR $\rightarrow$ 256 CBNR-MP $\rightarrow$ 256 CBNR $\rightarrow$ 512 CBNR-MP $\rightarrow$ 512 CBNR $\rightarrow$ 1024 CBNR-MP; the feature extractor of c is composed of three Fully Connection-Batch Normalization-ReLU (FC-BNR) blocks with structure 128 $\rightarrow$ 256 $\rightarrow$ 512. The concatenated features are further transformed by four 64 FC-BNR to generate $\mu_{s,z}(x, d_s)$ and $\log \sigma_{s,z}(x, d_s)$. For the prior model $p_\theta(s, z|d_s)$, it shares the same structure without feature extractor of x. For $p_\phi(x|s, z)$, the network is composed of three DeConvolution-Batch Normalization-ReLU (DCBNR) blocks and three Convolution-Batch Normalization-ReLU (CBNR) blocks, followed by a convolutional layer, with structure 256 DCBNR $\rightarrow$ 256 CBNR $\rightarrow$ 128 DCBNR $\rightarrow$ 128 CBNR $\rightarrow$ 64 DCBNR $\rightarrow$ 64 CBNR $\rightarrow$ 48 Conv. For $p_\phi(y|s)$, the network is composed of 256 FC-BNR $\rightarrow$ 512 FC-BNR $\rightarrow$ 3 FC-BNR. For prior model $p_\phi(s, z|d_s)\mathcal{N}(\mu_{s,z}(d_s), \text{diag}(\sigma^2_{s,z}(d_s)))$ the $\mu_{s,z}(x, d_s)$ and $\log \sigma_{s,z}(x, d_s)$ are parameterized by Multi Perceptron Neural Network (MLP). The decoders $p_\phi(x|s, z)$ are $p_\phi(y|s)$ parameterized by Deconvolutional neural network. For all methods, we train for 200 epochs using SGD with weight decay 2×10^{-4} and learning rate 0.01 and is multiplied by 0.2 after every 60 epochs. The batch size is set to 4. For each variable in biomarker vector $C \in \mathbb{R}^9$, each person may have multiple records, and we take its median as representative to avoid extreme values due to device abnormality.

As for LaCIM-d, we adopt the same decoder $p_\phi(x|z, s)$ and classifier $p_\phi(y|s)$. For $q_\psi(s, z|x, d)$, we adopt the same network for the shared part; for the part specific to each domain, $\mu_{s,z}(x, d)$ and $\log \sigma_{s,z}(x, d)$ are generated by the sub-network which is composed of 1024 FC-BNR $\rightarrow$ 1024 FC-BNR $\rightarrow$ $q_{z,s}$ FC-BNR. The z, s can be reparameterized by $\mu_{s,z}(x, d)$ and $\log \sigma_{s,z}(x, d)$ are fed into a sub-network which is composed of $q_{z,s}$ FC-BNR $\rightarrow$ 1024 FC-BNR $\rightarrow$ $q_{z,s}$ FC-BNR to get rid of the constraint of Gaussian distribution. Then the reconstructed images and predicted label are computed by $p_\phi(x|z, s)$ and $p_\phi(y|s)$ which have the same network structure of LaCIM-C with the z, s.

Table 10: Training and test environments (characterized by c) in early prediction of AD

	Training Env#1	Training Env#1	Test
	Age		
Number of AD	17	17	14
Number of MCI	76	83	35
Number of NC	34	27	14
Average value of d_s (years):	68.75	72.78	81.74
	TAU		
Number of AD	11	22	15
Number of MCI	75	78	41
Number of NC	40	27	18
Average value of d_s:	215.34	286.69	471.72

The d_s variable in training and test. The selected attributes include Education Years, Age, Gender (0 denotes male and 1 denotes female), AV45, amyloid$_\beta$ and TAU. We split the data into $m = 2$ training environments and test according to different value of d_s. The Tab. 7.13 describes the data distribution in terms of number of samples, the value of d_s (Age and TAU).

7.13.1 Experiments with Complete Observable Source Variable

In image-based diagnosis, the personal attributes, genes and biomarkers are often available. Therefore, we consider the setting when d_s can be fully observed. In this case, the value of d_s is person-by-person. Therefore, the number of environments m is equal to the number of samples. In this case, the dataset turns to $\{x_i, y_i, d_s^i\}_{i=1}^n$. The expected risk turns to:

$$\mathcal{L}_{\psi,\phi} = \mathbb{E}_{p(x,y|d_s)}\left[-\log q_\psi(y|x,d_s) - \mathbb{E}_{q_\psi(s,z|x,d_s)}\left[\frac{p_\phi(y|s)}{q_\psi(y|x,d_s)}\log\frac{p_\phi(x|s,z)p_\phi(s,z|d_s)}{q_\psi(s,z|x,d_s)}\right]\right]. \tag{73}$$

And the corresponding empirical risk is:

$$\tilde{\mathcal{L}}_{\psi,\phi} = \frac{1}{n}\left[-\log q_\psi(y_i|x_i,d_{s,i}) - \mathbb{E}_{q_\psi(s,z|x_i,d_{s,i})}\left[\frac{q_\psi(y_i|s)}{q_\psi(y_i|x_i,d_{s,i})}\log\frac{p_\phi(x_i|s,z)p_\phi(s,z|d_{s,i})}{q_\psi(s,z|x_i,d_{s,i})}\right]\right]. \tag{74}$$

The d_s here is re-defined as the 9-dimensional vector that includes all attributes, genes and biomarkers mentioned above. We re-split the data into 80% train and 20% test, according to different average value of specific variable in the whole vector d_s.

The d_s variable in training and test We implemented OOD tasks in which the value of d_s is different between training and test. Specifically, we repeatedly split the dataset into the training and the test according to a selected attribute in d_s for three times. The average value of these attributes in train and test are recorded in Table 7.13.1.

Experimental Results We conduct OOD experiments with source variables Age, Gender, amyloid$_\beta$ and TAU different between training data and the test. The results are shown in Table 12.

7.14 Supplementary for Deepfake

Implementation Details. We implement data augmentations, specifically images with 30 angle rotation, with flipping horizontally with 50% probability. We additionally apply random compressing techniques, such as JpegCompression. For inference model, we adopt Efficient-B5 Tan and Le (2019), with the detailed network structure as: FC(2048, 2048) $\rightarrow$ BN $\rightarrow$ ReLU $\rightarrow$ FC(2048, 2048) $\rightarrow$ BN $\rightarrow$ ReLU $\rightarrow$ FC(2048, $q_{t=s,z}$). The structure of reparameterization, *i.e.*, $\rho_{t=s,z}$ is FC($q_{t=s,z}$, 2048) $\rightarrow$ BN $\rightarrow$ ReLU $\rightarrow$ FC(2048, 2048) $\rightarrow$ BN $\rightarrow$ ReLU $\rightarrow$ FC(2048, $q_{t=s,z}$). The network structure for generative model, *i.e.*, $p_\psi(x|s,z)$ is TConv-BN-ReLU($q_{t=s,z}$, 256) $\rightarrow$ TConv-BN-ReLU(256, 128) $\rightarrow$ TConv-BN-ReLU(128, 64)$\rightarrow$ TConv-BN-ReLU(64, 32) $\rightarrow$ TConv-BN-ReLU(32, 32) $\rightarrow$ TConv-BN-ReLU(32, 16) $\rightarrow$ TConv-BN-ReLU(16, 16) $\rightarrow$ Conv-BN-ReLU(16, 3) $\rightarrow$ Sigmoid,

Table 11: Training and test environments (characterized by c) in early prediction of AD

	Education Years	Age	Gender (0/1)	AV45	amyloid$_\beta$	TAU
	Setting #1					
Training	15.34	70.56	1.29	1.21	745.61	249.38
Test	19.44	81.74	1.83	1.56	1322.47	471.72
	Setting #2					
Training	15.34	70.62	1.29	1.21	743.01	250.21
Test	19.43	81.19	1.83	1.57	1332.94	446.67
	Setting #3					
Training	15.34	70.62	1.29	1.21	743.39	254.7
Test	19.44	81.19	1.83	1.56	1331.4	446.9

Table 12: Accuracy (%) of OOD prediction on ADNI. Average over three runs.

ACC (%) / Method	Setting#1	Setting#2	Setting#3	Setting#1	Setting#2	Setting#3
OOD source	Education Years			AV45		
CE $X \to Y$	61.9 ± 0.0	66.7 ± 1.6	63.0 ± 0.9	67.7 ± 0.9	66.1 ± 3.3	66.1 ± 1.8
DANN	62.4 ± 0.9	62.4 ± 0.9	63.0 ± 1.8	64.6 ± 0.9	67.2 ± 0.9	66.1 ± 0.9
CE $(X, d_s) \to Y$	67.2 ± 1.8	66.7 ± 3.2	63.0 ± 1.8	66.1 ± 3.3	66.1 ± 1.8	64.0 ± 0.9
sVAE	67.2 ± 0.9	67.2 ± 0.9	67.2 ± 0.9	65.6 ± 1.8	66.7 ± 2.7	65.1 ± 1.6
LaCIM-d_s (**Ours**)	$\mathbf{69.8 \pm 1.6}$	$\mathbf{68.8 \pm 0.9}$	$\mathbf{69.8 \pm 1.6}$	$\mathbf{69.3 \pm 1.8}$	$\mathbf{67.7 \pm 0.9}$	$\mathbf{67.7 \pm 0.0}$
OOD source	Age			Gender		
CE $X \to Y$	63.6 ± 2.6	65.6 ± 6.0	64.8 ± 4.7	60.5 ± 0.9	60.5 ± 1.8	60.5 ± 0.9
DANN	60.8 ± 1.8	58.7 ± 0.0	58.7 ± 0.0	58.5 ± 1.5	61.5 ± 0.0	60 ± 1.5
CE $(X, d_s) \to Y$	60.4 ± 2.9	64.5 ± 2.4	64.4 ± 3.8	63.2 ± 0.9	65.6 ± 1.8	64.1 ± 0.9
sVAE	58.2 ± 0.9	60.0 ± 1.8	58.7 ± 1.6	64.1 ± 0.9	65.6 ± 1.8	64.1 ± 0.9
LaCIM-d_s (**Ours**)	$\mathbf{64.0 \pm 2.4}$	$\mathbf{70.4 \pm 2.4}$	$\mathbf{66.1 \pm 3.7}$	$\mathbf{65.6 \pm 0.9}$	$\mathbf{67.2 \pm 1.8}$	$\mathbf{68.2 \pm 0.9}$
ACC (%) / Method	Setting#1	Setting#2	Setting#3	Setting#1	Setting#2	Setting#3
OOD source	amyloid$_\beta$			TAU		
CE $X \to Y$	59.2 ± 0.9	63.5 ± 4.2	63.1 ± 5.1	64.6 ± 0.9	64.1 ± 0.0	66.0 ± 1.1
DANN	60.8 ± 0.9	60.8 ± 0.9	60.8 ± 0.9	64.6 ± 0.9	65.1 ± 0.9	64.6 ± 0.9
CE $(X, d_s) \to Y$	64.6 ± 1.8	64.6 ± 3.7	64.2 ± 2.4	64.6 ± 0.9	66.7 ± 0.9	67.0 ± 1.3
sVAE	66.1 ± 0.9	64.6 ± 0.9	63.5 ± 3.2	68.2 ± 0.9	68.8 ± 2.7	67.2 ± 1.6
LaCIM-d_s (**Ours**)	$\mathbf{68.3 \pm 1.6}$	$\mathbf{66.1 \pm 1.8}$	$\mathbf{65.6 \pm 2.4}$	$\mathbf{69.8 \pm 0.9}$	$\mathbf{71.4 \pm 1.8}$	$\mathbf{68.8 \pm 0.0}$

followed by cropping the image to the same size $3 \times 224 \times 224$. We set $q_{t=s,z}$ as 1024. We implement SGD as optimizer, with learning rate 0.02, weight decay 0.00005, and run for 9 epochs.

Table 13: General framework table for our method and baselines on $\mathrm{Data} \in \{\text{CMNIST}, \text{NICO}, \text{ADNI}, \text{DeepFake}\}$ Dataset. We denote the dimension of z or zs as $\dim_{z,zs}$. We list the output dimension (*e.g.* the channel number) of each module, if it is different from the one in Tab. 14.

Method / Dataset	CE $X \to Y$	CE $X, d \to Y$	MMD-AAE	DANN	DIVA	LaCIM-d_s	LaCIM-d
Data:CMNIST	$\mathrm{Enc}_x^{\mathrm{Data}}$ FC(256,$\dim_z$) Dec-CE$_y^{\mathrm{Data}}$	$\mathrm{Enc}_x^{\mathrm{Data}}$;$\mathrm{Enc}_d^{\mathrm{Data}}$ FC(512,$\dim_z$) Dec-CE$_y^{\mathrm{Data}}$	$\mathrm{Enc}_x^{\mathrm{Data}}$ FC-BN-ReLU(256,256) FC(256,256) $\to z$ $\mathrm{Dec}_y^{\mathrm{Data}}$; $\mathrm{Dec}_x^{\mathrm{Data}}$	$\mathrm{Enc}_x^{\mathrm{Data}}$ DANN-CLS$_y^{\mathrm{Data}}$; DANN-CLS$_y^{\mathrm{Data}}$	$p_\theta^{\mathrm{Data}}(x\|z_d, z_x, z_y)$ $p_{\theta_d}^{\mathrm{Data}}(z_d\|d)$ $p_{\theta_y}^{\mathrm{Data}}(z_y\|y)$ $q_{\phi_d}^{\mathrm{Data}}(z_d\|x)$ $q_{\phi_x}^{\mathrm{Data}}(z_x\|x)$ $q_{\phi_y}^{\mathrm{Data}}(z_y\|x)$	$\mathrm{Enc}_x^{\mathrm{Data}}$;$\mathrm{Enc}_d^{\mathrm{Data}}$ FC-BN-ReLU(512,256) FC(256,$\dim_{zs}$) $\mathrm{Dec}_y^{\mathrm{Data}}$;$\mathrm{Dec}_x^{\mathrm{Data}}$ prior: $\mathrm{Enc}_d^{\mathrm{Data}}$	$\mathrm{Enc}_x^{\mathrm{Data}}$ $\mathrm{Enc}_{z,s}^{\mathrm{Data}} \times m$ $\Phi_{z,s}^{\mathrm{Data}} \times m$ $\mathrm{Dec}_y^{\mathrm{Data}}$;$\mathrm{Dec}_x^{\mathrm{Data}}$
# of Params	1.12M	1.16M	1.23M	1.1M	1.69M	1.09M	0.92M
hyper-Params	lr: 0.1 wd:0.00005	lr: 0.2 wd: 0.0005	lr: 0.01 wd: 0.0001	lr: 0.1 wd: 0.0002	lr: 0.001 wd: 0.00001	lr: 0.1 wd: 0.0001	lr: 0.01 wd: 0.0002
Data:NICO	$\mathrm{Enc}_x^{\mathrm{Data}}$ FC(1024,$\dim_z$) Dec-CE$_y^{\mathrm{Data}}$	$\mathrm{Enc}_x^{\mathrm{Data}}$;$\mathrm{Enc}_d^{\mathrm{Data}}$ FC(512,$\dim_z$) Dec-CE$_y^{\mathrm{Data}}$	$\mathrm{Enc}_x^{\mathrm{Data}}$ FC-BN-ReLU(1024,1024) FC(1024,1024) $\to z$ $\mathrm{Dec}_y^{\mathrm{Data}}$; $\mathrm{Dec}_x^{\mathrm{Data}}$	$\mathrm{Enc}_x^{\mathrm{Data}}$ DANN-CLS$_y^{\mathrm{Data}}$; DANN-CLS$_y^{\mathrm{Data}}$	$p_\theta^{\mathrm{Data}}(x\|z_d, z_x, z_y)$ $p_{\theta_d}^{\mathrm{Data}}(z_d\|d)$ $p_{\theta_y}^{\mathrm{Data}}(z_y\|y)$ $q_{\phi_d}^{\mathrm{Data}}(z_d\|x)$ $q_{\phi_x}^{\mathrm{Data}}(z_x\|x)$ $q_{\phi_y}^{\mathrm{Data}}(z_y\|x)$	$\mathrm{Enc}_x^{\mathrm{Data}}$;$\mathrm{Enc}_d^{\mathrm{Data}}$ FC(1536,$\dim_{zs}$) $\mathrm{Dec}_y^{\mathrm{Data}}$;$\mathrm{Dec}_x^{\mathrm{Data}}$ prior: $\mathrm{Enc}_d^{\mathrm{Data}}$	$\mathrm{Enc}_x^{\mathrm{Data}}$ $\mathrm{Enc}_{z,s}^{\mathrm{Data}} \times m$ $\Phi_{z,s}^{\mathrm{Data}} \times m$ $\mathrm{Dec}_y^{\mathrm{Data}}$;$\mathrm{Dec}_x^{\mathrm{Data}}$
# of Params ($m = 8$)	18.08M	19.01M	19.70M	19.13M	14.86M	16.31M	18.25M
# of Params ($m = 14$)	18.08M	19.01M	19.70M	26.49M	14.87M	18.08M	19.70M
hyper-Params	lr: 0.01 wd: 0.0002	lr: 0.01 wd: 0.0002	lr: 0.2 wd: 0.0001	lr: 0.05 wd: 0.0005	lr: 0.001 wd: 0.0001	lr: 0.01 wd: 0.0005	lr: 0.01 wd: 0.0001
Data:ADNI	$\mathrm{Enc}_x^{\mathrm{Data}}$ FC(1024,$\dim_z$) Dec-CE$_y^{\mathrm{Data}}$	$\mathrm{Enc}_x^{\mathrm{Data}}$;$\mathrm{Enc}_d^{\mathrm{Data}}$ FC(1536,$\dim_z$) Dec-CE$_y^{\mathrm{Data}}$	$\mathrm{Enc}_x^{\mathrm{Data}}$ FC-BN-ReLU(1024,1024) FC(1024,1024) $\to z$ $\mathrm{Dec}_y^{\mathrm{Data}}$; $\mathrm{Dec}_x^{\mathrm{Data}}$	$\mathrm{Enc}_x^{\mathrm{Data}}$ DANN-CLS$_y^{\mathrm{Data}}$; DANN-CLS$_y^{\mathrm{Data}}$	$p_\theta^{\mathrm{Data}}(x\|z_d, z_x, z_y)$ $p_{\theta_d}^{\mathrm{Data}}(z_d\|d)$ $p_{\theta_y}^{\mathrm{Data}}(z_y\|y)$ $q_{\phi_d}^{\mathrm{Data}}(z_d\|x)$ $q_{\phi_x}^{\mathrm{Data}}(z_x\|x)$ $q_{\phi_y}^{\mathrm{Data}}(z_y\|x)$	$\mathrm{Enc}_x^{\mathrm{Data}}$;$\mathrm{Enc}_d^{\mathrm{Data}}$ FC(1536,$\dim_{zs}$) $\mathrm{Dec}_y^{\mathrm{Data}}$;$\mathrm{Dec}_x^{\mathrm{Data}}$ prior: $\mathrm{Enc}_d^{\mathrm{Data}}$	$\mathrm{Enc}_x^{\mathrm{Data}}$ $\mathrm{Enc}_{z,s}^{\mathrm{Data}} \times m$ $\Phi_{z,s}^{\mathrm{Data}} \times m$ $\mathrm{Dec}_y^{\mathrm{Data}}$;$\mathrm{Dec}_x^{\mathrm{Data}}$
# of Params	28.27M	28.27M	36.68M	30.21M	33.22M	33.07M	37.78M
hyper-Params	lr: 0.01 wd: 0.0002	lr: 0.01 wd: 0.0002	lr: 0.005 wd: 0.0002	lr: 0.01 wd: 0.0002	lr: 0.005 wd: 0.0001	lr: 0.005 wd: 0.0002	lr: 0.01 wd: 0.0002

Table 14: Network Structure of Modules used in our method and baselines.

Method	CMNIST	NICO	ADNI
$\text{Enc}_x^{\text{Data}}$	Conv-BN-ReLU($\text{dim}_{\text{input}}$,64,3,1,1) MaxPool(2) Conv-BN-ReLU(64,128,3,1,1) MaxPool(2) Conv-BN-ReLU(128,256,3,1,1) MaxPool(2) Conv-BN-ReLU(256,256,3,1,1) AdaptivePool(1) Flatten()	Conv-BN-ReLU($\text{dim}_{\text{input}}$,128,3,1,1) Conv-BN-ReLU(128,256,3,2,0) MaxPool(2) Conv-BN-ReLU(256,256,3,1,1) Conv-BN-ReLU(256,512,3,1,1) MaxPool(2) Conv-BN-ReLU(512,512,3,1,1) Conv-BN-ReLU(512,512,3,1,1) MaxPool(2) Conv-BN-ReLU(512,512,3,1,1) Conv-BN-ReLU(512,1024,3,1,1) AdaptivePool(1) Flatten()	Conv3d-BN-ReLU($\text{dim}_{\text{input}}$,128,3,1,1) Conv3d-BN-ReLU(128,256,3,2,0) MaxPool(2) Conv3d-BN-ReLU(256,256,3,1,1) Conv3d-BN-ReLU(256,512,3,1,1) MaxPool(2) Conv3d-BN-ReLU(512,512,3,1,1) Conv3d-BN-ReLU(512,512,3,1,1) MaxPool(2) Conv3d-BN-ReLU(512,512,3,1,1) Conv3d-BN-ReLU(512,1024,3,1,1) AdaptivePool(1) Flatten()
$\text{Dec}_x^{\text{Data}}$	UnFlatten() Upsample(2) Tconv-BN-ReLU($\text{dim}_{\text{input}}$,128,2,2,0) Tconv-BN-ReLU(128,64,2,2,0) Tconv-BN-ReLU(64,32,2,2,0) Tconv-BN-ReLU(32,16,2,2,0) Conv(16,3,3,1,1) Sigmoid() Cropping(28)	UnFlatten() Upsample(16) Tconv-BN-ReLU($\text{dim}_{\text{input}}$,256,2,2,0) Conv-BN-ReLU(256,256,3,1,1) Tconv-BN-ReLU(256,128,2,2,0) Conv-BN-ReLU(128,128,3,1,1) Tconv-BN-ReLU(128,64,2,2,0) Conv-BN-ReLU(64,64,3,1,1) Tconv-BN-ReLU(64,32,2,2,0) Conv-BN-ReLU(32,32,3,1,1) Conv(32,3,3,1,1) Sigmoid()	UnFlatten() Upsample(6) Tconv3d-BN-ReLU($\text{dim}_{\text{input}}$,256,2,2,0) Conv3d-BN-ReLU(256,256,3,1,1) Tconv3d-BN-ReLU(256,128,2,2,0) Conv3d-BN-ReLU(128,128,3,1,1) Tconv3d-BN-ReLU(128,64,2,2,0) Conv3d-BN-ReLU(64,64,3,1,1) Tconv3d-BN-ReLU(64,64,2,2,0) Conv3d-BN-ReLU(64,64,3,1,1) Conv3d(64,1,3,1,1) Sigmoid()
$\text{Enc}_d^{\text{Data}}$	FC-BN-ReLU(d, 128) FC-BN-ReLU(128, 256)	FC-BN-ReLU(d, 256) FC-BN-ReLU(256, 512) FC-BN-ReLU(512, 512)	FC-BN-ReLU(d, 256) FC-BN-ReLU(256, 512) FC-BN-ReLU(512, 512)
$\text{Dec}_y^{\text{Data}}$	FC-BN-ReLU($\text{dim}_{z,s}$, 512) FC-BN-ReLU(512, 256) FC(256,2)	FC-BN-ReLU($\text{dim}_{z,s}$, 512) FC-BN-ReLU(512, 256) FC(256,2)	FC-BN-ReLU($\text{dim}_{z,s}$, 512) FC-BN-ReLU(512, 256) FC(256,2)
$\text{Dec-CE}_y^{\text{Data}}$	FC-BN-ReLU($\text{dim}_{z,s}$, 512) FC-BN-ReLU(512, 256) FC(256,2)	FC-BN-ReLU($\text{dim}_{z,s}$, 1024) FC-BN-ReLU(1024, 2048) FC(2048,2)	FC-BN-ReLU($\text{dim}_{z,s}$, 512) FC-BN-ReLU(512, 256) FC(256,2)
$\text{DANN-CLS}_y^{\text{Data}}$	FC-BN-ReLU(256, 32) FC-BN-ReLU(32, 2)	FC-BN-ReLU(1024, 2048) FC-BN-ReLU(2048, 2)	FC-BN-ReLU(1024, 1024) FC-BN-ReLU(1024, 2)
$\Phi_{z,s}^{\text{Data}}$	FC-ReLU($\text{dim}_{z,s}$, 256) FC-ReLU(256, $\text{dim}_{z,s}$)	FC-ReLU($\text{dim}_{z,s}$, 1024) FC-ReLU(1024, $\text{dim}_{z,s}$)	FC-ReLU($\text{dim}_{z,s}$, 1024) FC-ReLU(1024, $\text{dim}_{z,s}$)
$\text{Enc}_{z,s}^{\text{Data}}$	FC-ReLU(256, 256) FC-ReLU(256, $\text{dim}_{z,s}$)	FC-ReLU(1024, 1024) FC-ReLU(1024, $\text{dim}_{z,s}$)	FC-ReLU(1024, 1024) FC-ReLU(1024, $\text{dim}_{z,s}$)
$p_\theta^{\text{Data}}(x\|z_d, z_x, z_y)$	FC-BN-ReLU(1024) UnFlatten() Upsample(8) TConv-BN-ReLU(64,128,5,1,0) Upsample(24) TConv-BN-ReLU(128,256,5,1,0) Conv(256, 256*3,1,1,0)	FC-BN-ReLU(1024) UnFlatten() Upsample(16) TConv-BN-ReLU(64,128,5,1,0) Upsample(64) TConv-BN-ReLU(128,256,5,1,0) Upsample(256) Conv(256, 3,1,1,0)	FC-BN-ReLU(1024) UnFlatten() Upsample(8) TConv3d-BN-ReLU(16,64,5,1,0) Conv3d-BN-ReLU(64,128,3,1,1) Upsample(24) TConv3d-BN-ReLU(128,128,5,1,0) Conv3d-BN-ReLU(128,128,3,1,1) Upsample(48) Conv3d-BN-ReLU(128,32,3,1,1) Conv3d(32, 1,1,1,0)
$p_{\theta_d}^{\text{Data}}(z_d\|d)$ $p_{\theta_y}^{\text{Data}}(z_y\|y)$	FC-BN-ReLU($\text{dim}_{d,y}$, 64) FC(64,64); FC(64,64)	FC-BN-ReLU($\text{dim}_{d,y}$, 64) FC(64,64); FC(64,64)	FC-BN-ReLU($\text{dim}_{d,y}$, 64) FC(64,64); FC(64,64)
$q_{\phi_d}^{\text{Data}}(z_d\|x)$ $q_{\phi_x}^{\text{Data}}(z_x\|x)$ $q_{\phi_y}^{\text{Data}}(z_y\|x)$	Conv-BN-ReLU(3,32,5,1,0) MaxPool(2) Conv-BN-ReLU(32,64,5,1,0) MaxPool(2) Flatten() FC(1024, 64); FC(1024, 64) $\texttt{Data}$	Conv-BN-ReLU(3,32,3,2,1) MaxPool(2) Conv-BN-ReLU(32,64,3,2,1) MaxPool(2) Conv-BN-ReLU(64,64,3,2,1) MaxPool(2) Flatten() FC(1024, 64); FC(1024, 64) $\texttt{Data}$	Conv3d-BN-ReLU(1,64,3,2,1) Conv3d-BN-ReLU(64,128,3,1,1) MaxPool(3) Conv3d-BN-ReLU(128,256,3,1,1) Conv3d-BN-ReLU(256,256,3,1,1) MaxPool(2) Conv3d-BN-ReLU(256,256,3,1,1) Conv3d-BN-ReLU(256,128,3,1,1) MaxPool(2) Flatten() FC(1024, 64); FC(1024, 64) $\texttt{Data}$